# REPORT DOCUMENTATION PAGE

*Form Approved*
*OMB No. 0704-0188*

Public reporting burden for this collection of information is estimated to average 1 hour per response, including the time for reviewing instructions, searching existing data sources, gathering and maintaining the data needed, and completing and reviewing this collection of information. Send comments regarding this burden estimate or any other aspect of this collection of information, including suggestions for reducing this burden to Department of Defense, Washington Headquarters Services, Directorate for Information Operations and Reports (0704-0188), 1215 Jefferson Davis Highway, Suite 1204, Arlington, VA 22202-4302. Respondents should be aware that notwithstanding any other provision of law, no person shall be subject to any penalty for failing to comply with a collection of information if it does not display a currently valid OMB control number. **PLEASE DO NOT RETURN YOUR FORM TO THE ABOVE ADDRESS.**

| | | |
|---|---|---|
| **1. REPORT DATE** *(DD-MM-YYYY)*<br>June 2014 | **2. REPORT TYPE**<br>Technical Paper | **3. DATES COVERED** *(From - To)*<br>June 2014- July 2014 |

**4. TITLE AND SUBTITLE**

MODELING OF FUEL FILM COOLING ON CHAMBER HOT WALL

**5a. CONTRACT NUMBER**
In-House

**5b. GRANT NUMBER**

**5c. PROGRAM ELEMENT NUMBER**

**6. AUTHOR(S)**

A. Himansu, E.B. Coy, V. Sankaran, S.A. Danczyk

**5d. PROJECT NUMBER**

**5e. TASK NUMBER**

**5f. WORK UNIT NUMBER**
Q0VZ

**7. PERFORMING ORGANIZATION NAME(S) AND ADDRESS(ES)**

Air Force Research Laboratory (AFMC)
AFRL/RQRC
10 E. Saturn Blvd.
Edwards AFB CA 93524-7680

**8. PERFORMING ORGANIZATION REPORT NO.**

**9. SPONSORING / MONITORING AGENCY NAME(S) AND ADDRESS(ES)**
Air Force Research Laboratory (AFMC)
AFRL/RQR
5 Pollux Drive
Edwards AFB CA 93524-7048

**10. SPONSOR/MONITOR'S ACRONYM(S)**

**11. SPONSOR/MONITOR'S REPORT NUMBER(S)**
**AFRL-RQ-ED-TP-2014-233**

**12. DISTRIBUTION / AVAILABILITY STATEMENT**
Distribution A: Approved for Public Release; Distribution Unlimited

**13. SUPPLEMENTARY NOTES**
Technical paper and presentation presented at 50th AIAA/ASME/SAE/ASEE Joint Propulsion Conference, Cleveland, OH, 28-30 July, 2014. PA#14402

**14. ABSTRACT**

A steady Reynolds-averaged Navier-Stokes model with multiple species, conjugate heat transfer and equilibrium chemistry is constructed to simulate hydrocarbon fuel film cooling of the hot-gas side of liquid rocket engine chamber walls. The predictive performance of the model is studied by comparison to experimental heat flux data for several flow conditions and film cooling mass flow rates. Physics and chemistry aspects are identified that are either not modeled in sufficient detail in the current model or the representation of which otherwise involves uncertainty. The sensitivity of the wall heat flux to these factors is evaluated by perturbing the corresponding parameters and conditions in the model. A key finding is that, under the conditions of the experiments used for comparison, radiative heat flux is comparable to convective heat flux upstream of the injection slot. The sensitivity studies show that the other major factors potentially affecting the heat flux are soot formation accompanied by the deposit of a thermal barrier coating of carbon on the wall, and the magnitude of turbulent mass diffusivity in supercritical high-density ratio shear layers.

**15. SUBJECT TERMS**

| | | | | | |
|---|---|---|---|---|---|
| **16. SECURITY CLASSIFICATION OF:** | | | **17. LIMITATION OF ABSTRACT** | **18. NUMBER OF PAGES** | **19a. NAME OF RESPONSIBLE PERSON**<br>E. Coy |
| **a. REPORT**<br>**Unclassified** | **b. ABSTRACT**<br>**Unclassified** | **c. THIS PAGE**<br>**Unclassified** | SAR | 67 | **19b. TELEPHONE NO** *(include area code)*<br>661-275-5219 |

**Standard Form 298 (Rev. 8-98)**
**Prescribed by ANSI Std. 239.18**

# Modeling of Fuel Film Cooling on Chamber Hot Wall

Ananda Himansu[1], Edward B. Coy[2], Venkateswaran Sankaran[3] and Steven A. Danczyk[4]
*Air Force Research Laboratory, Edwards AFB, CA, 93524*

**A steady Reynolds-averaged Navier-Stokes model with multiple species, conjugate heat transfer and equilibrium chemistry is constructed to simulate hydrocarbon fuel film cooling of the hot-gas side of liquid rocket engine chamber walls. The predictive performance of the model is studied by comparison to experimental heat flux data for several flow conditions and film cooling mass flow rates. Physics and chemistry aspects are identified that are either not modeled in sufficient detail in the current model or the representation of which otherwise involves uncertainty. The sensitivity of the wall heat flux to these factors is evaluated by perturbing the corresponding parameters and conditions in the model. A key finding is that, under the conditions of the experiments used for comparison, radiative heat flux is comparable to convective heat flux upstream of the injection slot. The sensitivity studies show that the other major factors potentially affecting the heat flux are soot formation accompanied by the deposit of a thermal barrier coating of carbon on the wall, and the magnitude of turbulent mass diffusivity in supercritical high-density ratio shear layers.**

## Nomenclature

*2-D* = two-dimensional
$d$ = streamwise length of FFC slot
$x$ = streamwise Cartesian coordinate
$y$ = wall-normal Cartesian coordinate
$y^+$ = dimensionless $y$-spacing at wall
CEA = Chemical Equilibrium with Applications (computer program)
CFD = Computational Fluid Dynamics
CMFR = Core Mass Flow Rate
FFC = Fuel Film Cooling
M&S = Modeling and Simulation
PDE = Partial Differential Equation
PDF = Probability Distribution Function
RANS = Reynolds-averaged Navier-Stokes
RFL = Rich Flammability Limit
RP-2 = Rocket Propellant-2

## I. Introduction

The walls of liquid rocket engine chambers and nozzles must contain large pressures while being exposed to very high temperature gases, and therefore must be cooled to maintain their structural integrity. The two main technologies used to keep the walls cool are (a) rapid heat removal by flowing cool fuel through channels embedded in the walls, and (b) shielding of the wall from hot gases by injection of cool fuel or oxidizer film along the wall. In the pursuit of higher power density, rocket engine designers are now considering greater propellant mass fluxes than in previous designs. This results in higher heat fluxes to engine walls, such that the walls cannot be sufficiently cooled by embedded regenerative fuel coolant technology alone, making film cooling essential. The high reactivity

---

Distribution A: Authorized for public release, distribution unlimited.
[1] Aerospace Engineer, Combustion Devices Branch.
[2] Mechanical Engineer, Combustion Devices Branch, Senior Member, AIAA.
[3] Senior Scientist, Aerospace Systems Directorate, Senior Fellow, AIAA.
[4] Research Scientist, Combustion Devices Branch, Member, AIAA.

of the oxidizer with the metal walls usually means that fuel must be used as the film coolant. The current study represents the initial step in a hydrocarbon fuel film cooling (FFC) simulation and design optimization study.

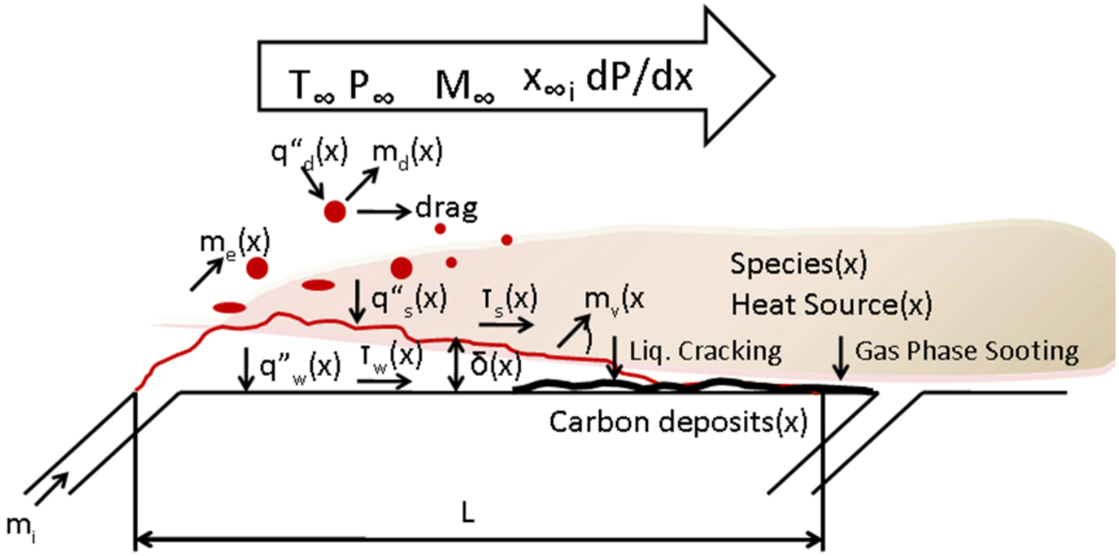

**Figure 1. Film cooling with a liquid hydrocarbon fuel.**

The physical and chemical phenomena involved in hydrocarbon FFC is notionally represented in Fig. 1. Hydrocarbon fuel at the fuel tank temperature is injected through a slot into a high-speed high-temperature turbulent reacting cross flow at supercritical pressure. The fuel jet and the cross-flow interact and part of the jet is stripped off and entrained by the hot gas. This portion disperses and mixes with the high-speed hot gas away from the wall, and does not contribute very much to cooling the wall. The rest of the jet is forced by momentum exchange to form a film on the wall, which serves to keep the wall cooler than in the absence of the film. The film is kept in motion along the wall by shear forces exerted by the hot gas, along with mutual exchange of mass, momentum and energy. As the fluid in the film heats up, it undergoes cracking or pyrolysis, and the resultant species undergo oxidation by the excess oxidizer diffusing from the hot cross flow. The pyrolysis produces a further cooling effect by its endothermic nature. When the products of pyrolysis diffuse into the hot gas, soot formation often occurs, followed by some soot destruction by oxidation. Some of the soot is also transported to the wall by turbulent mass diffusion, and surface chemistry and physics come into play, leading to carbonaceous deposits being formed on the wall. This carbon layer can further provide substantial wall protection by acting as a thermal barrier. Further downstream, when the film has been depleted of its cooling and coking capacities, a second slot is needed to inject fresh cool fuel. All of these processes pose great challenges to computational modeling. The supercritical pressures require the use of specialized equations of state, transport properties and mixture rules. The large temperature range causes large variations in fluid properties, reaction rates and composition. The detailed chemistry of hydrocarbon combustion, pyrolysis, soot formation, and soot oxidation can involve hundreds of species and thousands of reactions. The transport of soot particulates, and the surface physics and chemistry of wall deposition, and change of effective wall thermal resistance are also very complex to simulate numerically. Furthermore, radiative heat transfer through an absorbing-emitting medium, and conjugate heat transfer coupling the convective heat transfer in the fluid with the heat conduction occurring in the metal wall further complicate the modeling.

There is a substantial literature on the modeling and simulation of film cooling for gas turbine engines. In that area, the film is used to cool the turbine stator blades downstream of the combustor. The models do not usually involve chemical reactions, as the film fluid is air bled from the high-pressure compressor. The temperatures and pressures encountered are also not as extreme as those found in liquid rocket engines. There is also some literature on hydrogen film cooling modeling, but there has been limited attention paid to the modeling of hydrocarbon fuel film cooling at supercritical pressures. A relevant recent simulation study by Yang and Sun[1] used a finite-rate laminar chemistry approach, including the T.S. Wang kerosene combustion mechanism[2], to model kerosene film cooling and the attendant pyrolysis reactions. Their study did not attempt to validate the simulations with experimental data. Kirchberger, Schlieben and Haidn[3] used analytical and semi-empirical formulas to predict the cooling effect of films, and obtained comparison with experiment that they deemed unsatisfactory.

The current study is the first phase of the modeling and simulation (M&S) portion of a study to advance hydrocarbon FFC technology for liquid rocket engines. The goals of the M&S effort are to provide validated predictive physics-based simulation tools for design optimization of FFC. Design optimization would involve tailoring the FFC injection slot spacing and the FFC mass and momentum fluxes to provide adequate wall protection while minimizing the loss of specific impulse due to partial and non-optimal fuel combustion. The approach taken in this effort is to construct a model of the FFC physics and chemistry using the best available codes and models. We then evaluate the strengths and weaknesses of the model by validating the predicted results using lab-scale experimental data, and performing numerical sensitivity studies for model elements for which there is significant uncertainty regarding accuracy.

## II. Validation Cases

Numerical simulations were performed for cases corresponding to experiments performed in our laboratory. In the experiments, the gas flow-path from the injector face to the to the test section of the bench-scale combustor includes an acoustic cavity section, an igniter section, a straight section square cross-section, that then transitions to a straight section of a smaller square cross-section, which in turn leads to the test section. Downstream of the measurement panel are a square-to-round transition section and a nozzle exhausting to the atmosphere. The walls of the entire flow-path are water-cooled with flow channels embedded in the metal walls.

The sizes and dimensions of the experimental arrangement and of the computational domain are listed in terms of d, the FFC slot "length" or streamwise extent. The heat flux measurement panel of the test article used in the experiments forms one of the four walls of the test section. The FFC slot extends across the width of the panel. The measurement panel extends 28.4*d* upstream of the slot and 121.2*d* downstream of it. The hot gases created by the primary combustion in the gas generator upstream of the test section flow over the panel. The portions of the panel both upstream and downstream of the slot house multiple water calorimeters, with water passages embedded beneath the panel surface and running parallel to the slot. Each calorimeter measures the panel surface heat flux averaged over its own exposed surface area. The calorimeters serve also to cool the wall and thereby preserve its structural integrity. RP-2 fuel was injected through the FFC slot from injection manifolds under the wall. The injected RP-2 provided film cooling of the exposed panel surface downstream of the slot.

A nominal chamber pressure of 700 psi was used for all cases. The mixture ratio was 2.8. Two different core mass flow rates (CMFR) were used, referred to as "large" and "small". With the large CMFR, in addition to a non-film-cooled case, cases corresponding to FFC mass flow rates of 0.6%, 1.5% and 2.9% of the CMFR were run. With the small CMFR, a non-FFC case as well as cases with FFC mass flow rates of 1.5%, 3% and 6% of the corresponding CMFR were run.

## III. Numerical Models and Simplifying Approximations

The physical modeling approach that we have taken begins with the simplest plausible model incorporating the physics known to be important in the FFC problem. We then performed preliminary simulations and evaluated the accuracy of the predictions for selected validation cases. We further performed numerical sensitivity studies to identify key aspects of the model that significantly influence the wall heat flux and that may need to be more accurately modeled. In this section, we describe the physical modeling choices used in this study.

First, we list and discuss the approximations we made in modeling both the fluid behavior and the constraints imposed in the experiments:

1. A Reynolds-averaged steady mean flow representation is used, and the effect of the fluid turbulence on the mean flow is approximated by including a Reynolds-averaged Navier-Stokes (RANS) turbulence model as part of the computational model.
2. The flow in the combustion chamber is assumed to be two-dimensional. This neglects the boundary-layer thickening at the edges formed by the corners of the square cross-section as well as the acceleration of the core flow caused by the thickening of the boundary layer on the side walls.
3. The FFC injection manifold is modeled by a straight duct of constant cross-section, with walls at right-angles to the test panel wall.
4. The detailed combustion process and flame downstream of the injector are not modeled in the run-up simulation. The entire process is instead represented by assuming the combustion to be complete at the injector face as predicted by a quasi-one-dimensional equilibrium chemistry calculation performed the Chemical Equilibrium with Applications (CEA) computer program of Ref. 4.

5. The fluid in the chamber was taken to be a mixture of the hot gases and the fuel injected via the FFC slot. Kerosene vapor was used as a simulant for the injected fuel. Ideal gas equations of state were used in both cases. For the results shown in this abstract, the transport properties of the mixture were taken to be constant and equal to those of the hot gas at 800 K, as predicted by CEA[4].
6. We assume that the mixture is in chemical equilibrium at all stages of the mixing between core flow and film. This is equivalent to assuming that the chemical reactions caused by the mixing of fuel and hot combustion products that include oxygen are much faster than the fluid convection. Such an approximation allows the use of a conserved scalar approach to accounting for changes in chemical composition, which is computationally cheaper than using finite-rate chemistry for the pyrolysis and oxidation.
7. As discussed in the introductory section, sooting and coking are notoriously complex topics. Well-validated global reduced kinetic mechanisms are needed to keep the computational cost within reason. In the current phase of this modeling effort, we have omitted accurate models for soot formation and deposition. Instead, the potential impact of the coke layer is evaluated parametrically by representing the thermal effect of the carbon deposition using a constant thermal resistance downstream of the injection slot.
8. The thermal boundary condition at the walls of the combustion chamber was not well-characterized in the experiment. We used a conjugate heat transfer simulation that includes the effect of the water-cooling embedded in the walls to reduce the uncertainty in the thermal state of the wall boundary.
9. The conjugate heat transfer simulations include heat conduction in the wall, but do not include the details of the water channels in the calorimeters and the heat transfer therein. Instead, the chamber wall is taken as being of a constant thickness corresponding to the depth of the middle of the water channels, and a constant convective heat transfer coefficient is applied at that boundary.
10. For the simulation involving radiative heat transfer, the radiation absorption coefficient was taken to be 40 per meter, which is reasonable for a sooty gas. The estimation of the mean absorption coefficient of gaseous mixtures, particularly if particulates such as soot are present, is a complex process, as seen in Chapter 10 of Modest[5], and was deferred to future work.
11. A symmetry boundary condition was imposed at the wall of the combustion chamber opposite the FFC slot. This was done to save computational effort of resolving the boundary layer on that wall. Because of the distance between upper and lower walls, this simplification should have relatively little effect on the interaction between the chamber core flow and the fuel film.

The computational model used in the study was assembled in the ANSYS Fluent 15 commercial CFD software. The RANS turbulence model used is the Shear Stress Transport (SST) k-ω model of Menter[6] in the solution-to-wall mode without the use of wall functions. As discussed previously, the fluid was modeled as a multi-species fluid with equilibrium chemistry. Fluid properties for the individual species present in the fluid mixture are available in the standard Fluent properties database. From the properties of the individual species, Fluent calculates thermodynamic properties of the mixture based on its composition and temperature. This leaves only the transport properties of the fluid mixture, namely the molecular (laminar) viscosity and the molecular thermal conductivity, as specifiable by the user when assembling the model. One of the simulations included a sub-model, the P1 radiation model, to account for radiative heat transfer. The fluid mixture was assumed to be a gray participating medium for radiation.

A conserved scalar approach is used to model the multi-species chemistry, wherein the n-1 PDEs for species conservation are replaced by just two PDEs, one for conservation of the mean mixture fraction, f, and another for conservation of the variance, f'. This is much less expensive than tracking n-1 species. Furthermore, there are no chemistry source terms in these conservation equations, and so the system is relatively well-conditioned. The mixture fraction f serves to distinguish between a 'fuel' species and an 'oxidizer' species. The variance f' arises from a probability distribution function (PDF) representation of the turbulent fluctuations of the instantaneous mixture fraction. The mean values of density, temperature and individual species mass fractions must be calculated from values of f, f' and the mean enthalpy, h. Fluent pre-computes these relationships and stores them in a look-up table of PDFs that is used during the flow simulation, i.e. while numerically solving the conservation PDEs. In the current model, this is done by using equilibrium thermochemistry methods and knowledge of the specific heat as a function of temperature. In obtaining mean values from relationships that apply to instantaneous values, Fluent uses an assumed-shape PDF termed the β-Function PDF (see Peters[7] for details).

To describe the spatial computational domain that was selected, we use two-dimensional rectangular Cartesian coordinates $x$ and $y$, with the streamwise "length" of the slot, $d$, as the unit of length. The film-cooled panel wall is located at $y$=0. The trailing edge of the FFC injection slot is located at $x$=0, i.e. at the origin. The computational domain is 45.44 units high and stretches from $x$=-461.17 to $x$=121.15. The FFC injection manifold is modeled as a straight duct perpendicular to the panel wall, as seen below the *x*-axis in Fig. 2, with a “height” which is five times its “length”. This is a sufficient distance for a well-formed boundary layer to develop and to allow for the capture of the recirculation region within the duct.

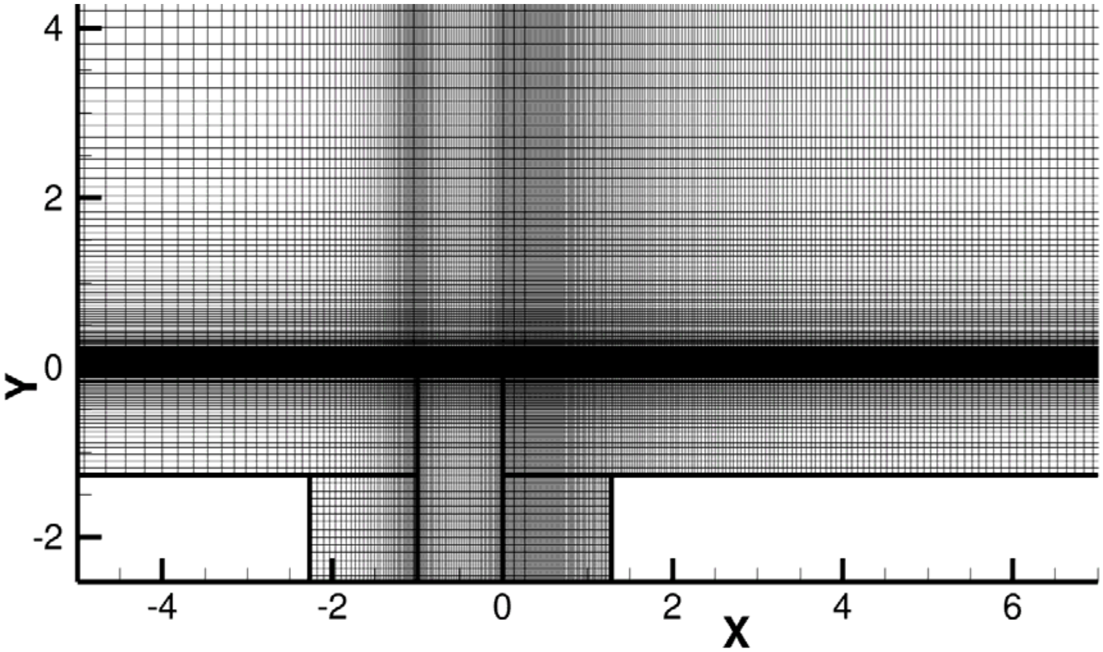

**Figure 2. Close-up view of mesh near slot.**

The mesh used for all simulations involving the FFC panel and an injection slot is a multi-block structured mesh with a total of about 173,000 quadrilateral cells. A close-up view near the slot is provided in Fig. 2, where the region of very fine *y*-spacing is the near-wall region. The vertical slot and the solid copper wall regions are seen below the wall surface. Near-wall mesh spacing was such that the wall-adjacent value of $y^+$ lay between 0.5 and 1 for all the simulations presented here. This spacing should be sufficient for the k-ω turbulence model to resolve the momentum boundary layer satisfactorily. The mesh in the solid copper walls conformed to the fluid domain mesh, as seen in Fig. 2. The mesh for the FFC panel without an injection slot is similar in resolution.

For all simulations, symmetry conditions were specified at the upper boundary and no-slip velocity conditions were specified at all other walls bordering a chamber fluid zone. The “free-stream” cooling water temperature was taken to be a constant 350K in the convective heat transfer boundary condition applied at the computational boundary of the copper walls. An exit pressure boundary condition with a uniform absolute pressure value of 717.7 psia was specified at the outlet for all simulations. The mass flow rate equal to the corresponding experimental setting is specified at the inlet, with the velocity assumed to be normal to the inlet and the velocity profile assumed uniform across the inlet. The inlet temperature profile for all cases was set as a constant value of 3680 K, obtained as the adiabatic flame temperature from a CEA[4] calculation of the baseline case. Turbulence at the inlet was specified as a default turbulent intensity of 5% of the dynamic pressure. The mass flow rates of the FFC flows were also set to the corresponding values from the experiments, and the FFC inlet temperature was set to be 305 K for all cases. The mixture fraction variance was taken to be zero at both fuel and oxidizer inlets.

For both the run-up and the panel section simulations, the conserved mixture-fraction formulation in the non-premixed combustion model requires specification of fuel and oxidizer compositions, in order to build the PDF look-up table. The fuel was specified as kerosene vapor, and the ‘oxidizer’ composition was specified from an equilibrium computation performed of the primary flow of the baseline case using CEA[4]. The ‘oxidizer’ composition used is given in terms of mass fraction as [h2]=0.0061, [o2]=0.04414, [oh]=0.05646, [co]=0.35386, [o]=0.0132, [h]=0.00142, [h2o]=0.23882 and [co2]=0.286 (the species are indicated by the chemical formula used to identify them in Fluent). The limit on number of species to consider when building the table was set to be 12. This resulted in the consideration of the additional species methane and a form of carbon among the product species. Trials with larger limits showed that further species are present with mass fractions of 10-7 or less. In the non-premixed combustion model with the conserved mixture fraction approach as implemented in Fluent, a parameter is available when building the PDF table, termed the Rich Flammability Limit (RFL). The RFL can be set by the user; in the current work, the RFL was set at its default value of 0.1. The RFL is the threshold of the local mixture fraction variable below which equilibrium chemistry will be used to calculate the composition and density of the mixture. For values of the mixture fraction larger than the RFL, the composition and density will be calculated by assuming pure mixing without chemical equilibrium between the state when the mixture fraction equals the RFL and the state of pure fuel. The molecular thermal conductivity of the multi-component fluid formed by any mixture of the 12 species was set to be 0.07383 W/m-K and its molecular coefficient of viscosity to be 3.7903x10-5 Pa-s. These are the values of the properties of the hot combustion products at 800K, as estimated using CEA[4]. The optical properties of the fluid mixture were set as follows: absorption coefficient = 40 per meter, scattering coefficient = 0, refractive index = 1.

The numerical scheme selected in Fluent to solve the model used second-order spatial finite-volume discretization. The CFD solver mode used to obtain the steady-state solution for all cases was the pseudo-transient relaxation method for the coupled pressure-based scheme, with automatic time step selection. The solution was considered converged when the residuals dropped by five or more orders of magnitude.

## IV. Results and Discussion

We present simulation results of the experiments and associated parametric analyses in this section. We begin by illustrating the characteristic features of the baseline simulations. Then we present comparison of simulation results with experimental data of the wall surface heat flux, the reduction of which is the key figure of merit of FFC effectiveness. Finally, we present results of sensitivity studies of uncertain factors in the model, and on this basis identify areas where improved modeling accuracy is most likely to improve the wall heat flux predictions.

All cases presented here have nominal conditions of a 700 psi chamber pressure and a mixture ratio of 2.8. The case with large CMFR and FFC=1.5% is regarded as a baseline case. Figs. 3 through 9 are flooded contour plots of field variables characterizing the numerical solution of the baseline case. In contour plots of variables other than temperature, the display of the solid walls is suppressed for clarity. Contour plots for the other simulation cases are not shown because they exhibit similar features.

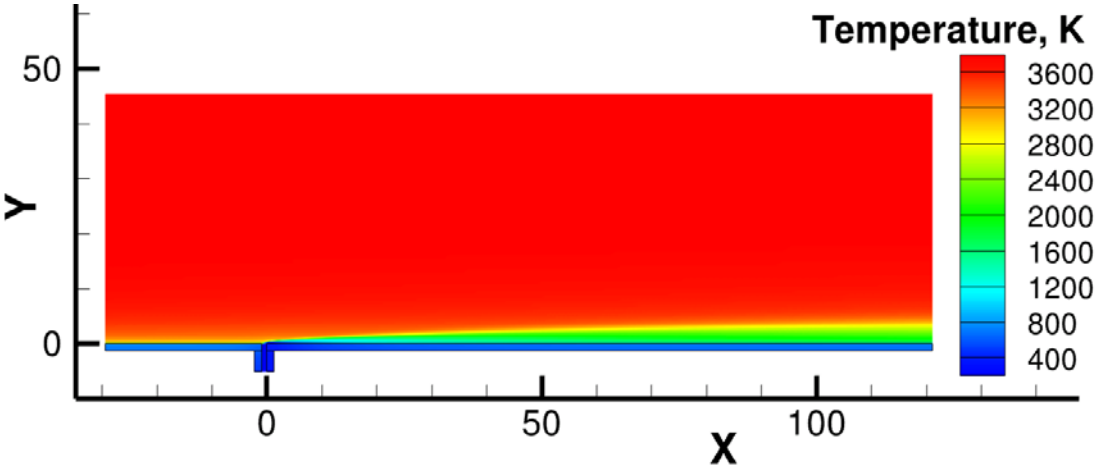

**Figure 3. Contours of temperature.**

The temperature field in the entire computational domain is shown in Fig. 3. The *x* coordinate is normalized by the FFC slot streamwise "length", and its origin is at the trailing edge of the FFC slot. The *y* coordinate is normalized in the same way, and its origin is at the hot surface of the test article wall. The solid copper chamber and slot walls are seen as blue bars at the bottom of the plot, and their temperature is generally under about 800K. In the vicinity of the chamber wall, downstream of the slot, we see the cooling effect produced by the injection of cool fuel at *x*=0 and its subsequent transport to the outlet downstream as a layer adjoining the wall. Note that temperatures in the film rise as the film fluid moves downstream, a result of mass and heat exchange with the hot core flow.

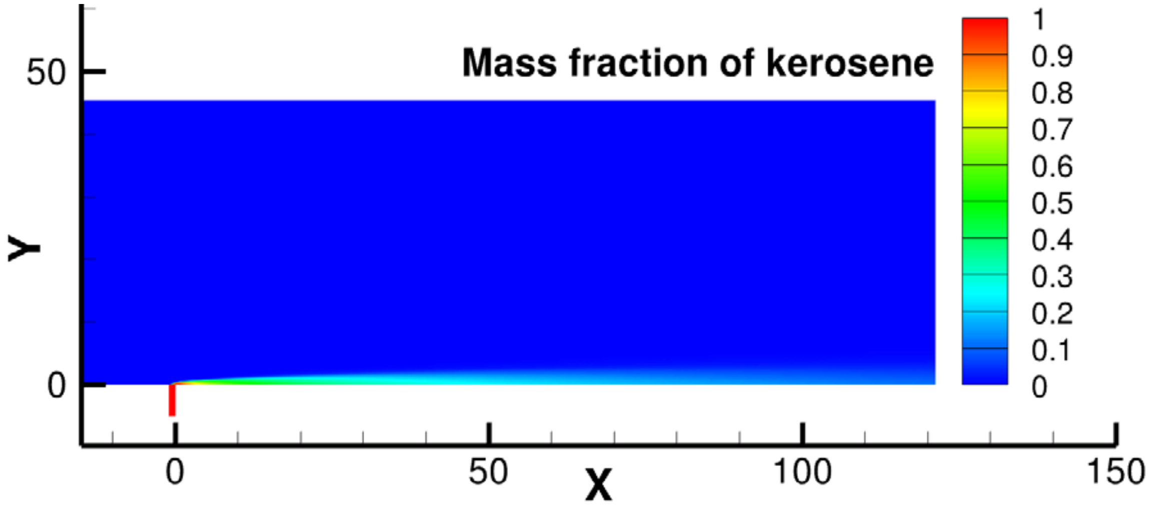

**Figure 4. Contours of mass fraction of kerosene.**

From the contours of the mass fraction of kerosene (the simulant for RP-2 used in these computations) in Fig. 4, we see that due to turbulent mass and heat exchange with the core flow, the equilibrium mass fraction of kerosene in the film decreases as it proceeds downstream. This is caused mostly by change in the chemical composition due to fuel pyrolysis as the film heats up, and to a lesser extent by turbulent mass diffusion of the kerosene away from the wall. This is also evident from comparison of Figs. 4 and 5. The mean mixture fraction in Fig. 5 shows that the matter originating in the kerosene stream persists much further downstream than the kerosene, gradually spreading out and thinning due to turbulent mass diffusion in the Y direction. The kerosene pyrolysis can be observed in the mass fraction contours of carbon monoxide in Fig. 6, in which the carbon monoxide is seen to reach a mass fraction of over 0.5 in the diffuse film at the test section exit. The composition transformations are spread across an appreciably thick layer between core flow and wall. This is the equivalent of a “reaction zone” within the current equilibrium chemistry model, and it is found to be not sharp but relatively thick.

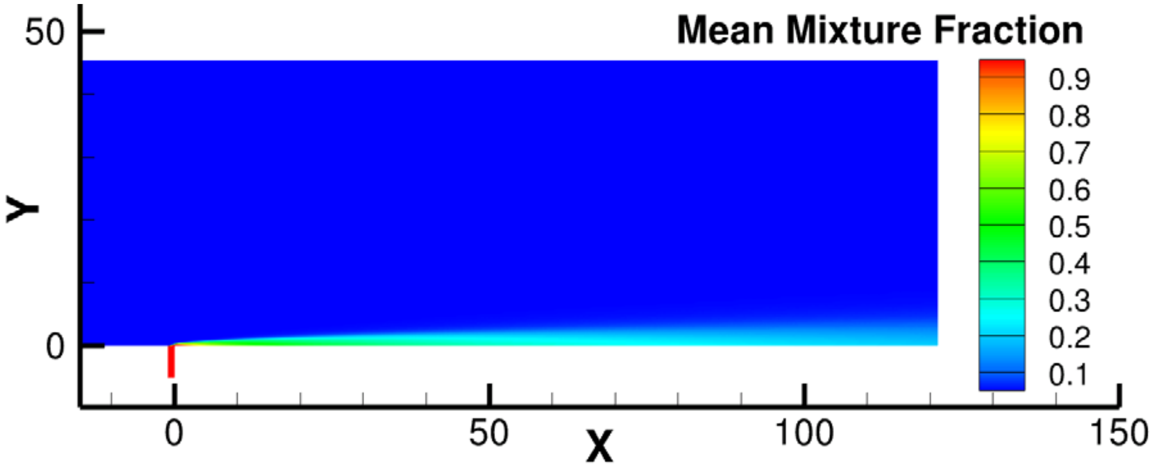

**Figure 5. Contours of mean mixture fraction.**

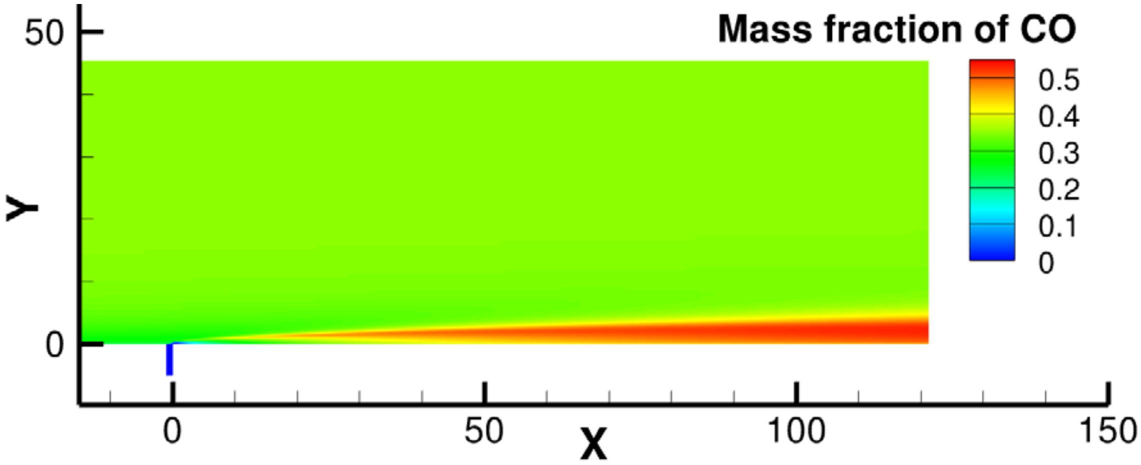

**Figure 6. Contours of mass fraction of carbon monoxide.**

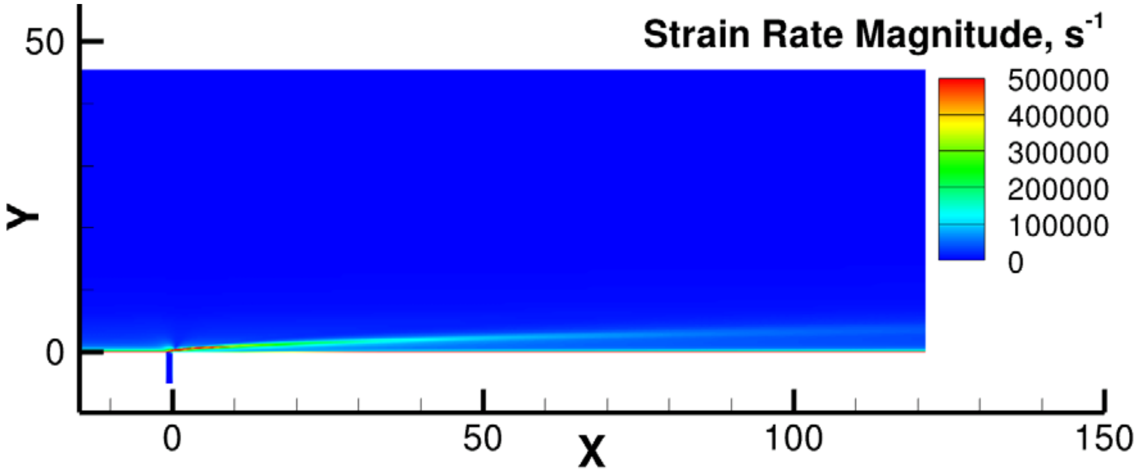

**Figure 7. Contours of strain-rate magnitude.**

Contours of the strain-rate magnitude in Fig. 7 show the presence of a shear layer between the fast-moving core flow and the slower wall film. The strain-rate values in units of "per second" show high levels of shear in the layer, which will significantly affect the turbulence in the film, though even higher shear exists between film and wall at the wall surface. The shear layers are regions of high strain-rate magnitude. Turbulent kinetic energy is created in the shear layer between core flow and film and is convected downstream.

Figs. 8 and 9 are contour plots viewed from close-up near the slot. Temperature contours in Fig. 8 show that the injected fuel jet does not penetrate very far from the wall, but is rapidly turned and forced to travel adjacent to the wall by the much larger momentum flux of the core flow. The copper walls downstream of the slot are seen to be cooler than upstream, due to the cooling effect of the injected kerosene.

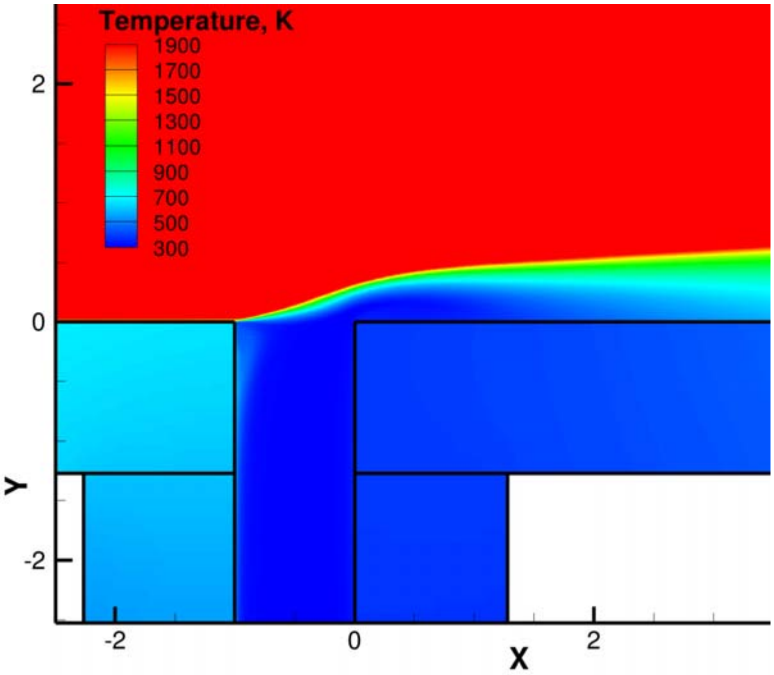

**Figure 8. Contours of temperature near slot.**

Density contours in Fig. 9 indicate that the density of the fuel vapor is only about a third of what is expected for 'liquid' kerosene at that high pressure. However, the mass flow rate and temperature of the injected fuel, which are the main factors in the cooling effect, are selected to match the experimental. The error in density causes an error in the injection velocity, but the cooling effect of the film is insensitive to this at such high momentum flux ratios between core flow and injected fuel. The overlaid streamlines show two recirculation regions, one within the injection manifold on the left wall and a larger one immediately downstream of the trailing edge of the slot. The second one will have a role in determining the level and distribution of turbulent kinetic energy within the wall film. The sizes of these recirculation regions are also observed to vary, depending on the FFC mass flow rate.

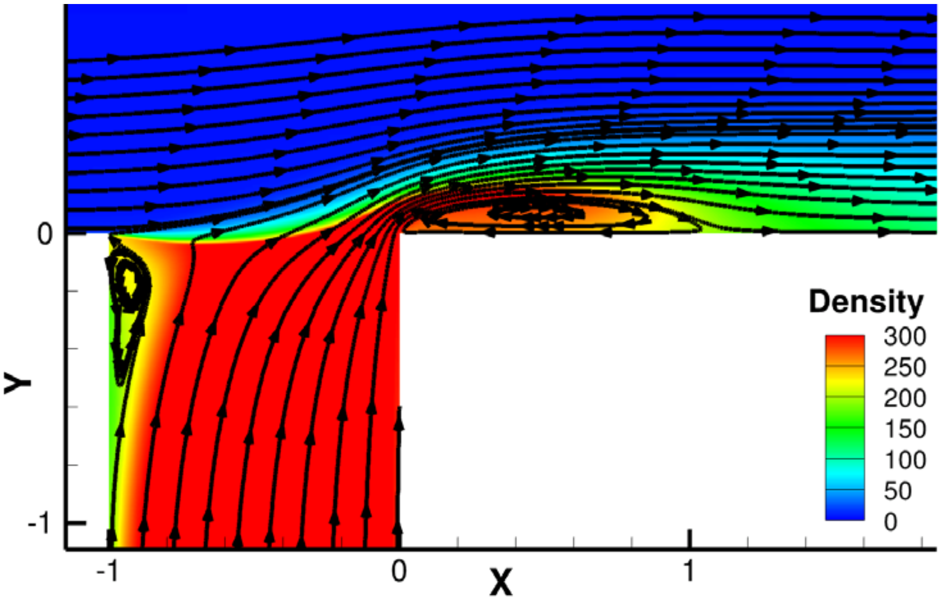

**Figure 9. Contours of density (kg/m$^3$) near slot, with streamlines.**

Figs. 10 through 20 are line plots comparing results of various simulations and available experimental data. All heat fluxes have been normalized with the value in the baseline simulation of the wall surface heat flux at the entry of the core flow into the test section.

The modeling simplifications in the development of the flow upstream of the test section lead to some uncertainty regarding the state of the fluid at the entrance to the test section, at $x$=-29.41. The uncertainty was dealt with by selecting the value of the convective heat transfer coefficient, h, on the copper walls such that the predicted heat flux for the large CMFR case without FFC matched the experimentally observed value at $x$=-9.41. This value of the coefficient h was thereafter used consistently without change across all simulations, together with a "freestream" cooling water temperature of 350K. The actual temperature of the cooling water rises by about 100K from its inlet to its outlet, but the value of 350K represents an average value between the inlet and outlet. The prediction results for different choices of h is reflected in Fig. 10. Also shown in Fig. 10 is the sensitivity of the surface heat flux in the simulation to the assumed value of h. It is seen that halving the value of h results in a significant reduction in wall heat flux. Moreover, an even greater heat flux reduction is predicted if the chemical equilibrium of the gas mixture making up the combusted gases at the inlet were frozen until the injected kerosene is encountered. The setting used instead for all the rest of the simulations is to allow the chemical equilibrium to adjust itself to the local temperature right from the inlet of hot gas and kerosene streams. The composition adjusts itself to lower-than-core temperatures in the boundary layer. Thereby, the heat flux is increased over the "frozen equilibrium" value.

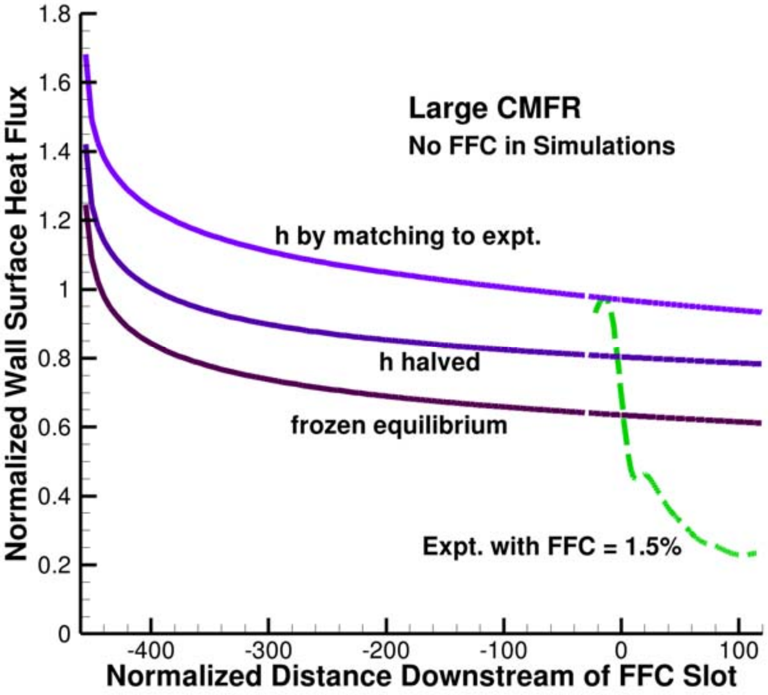

**Figure 10. Setting of heat transfer coefficient and equilibrium chemistry option.**

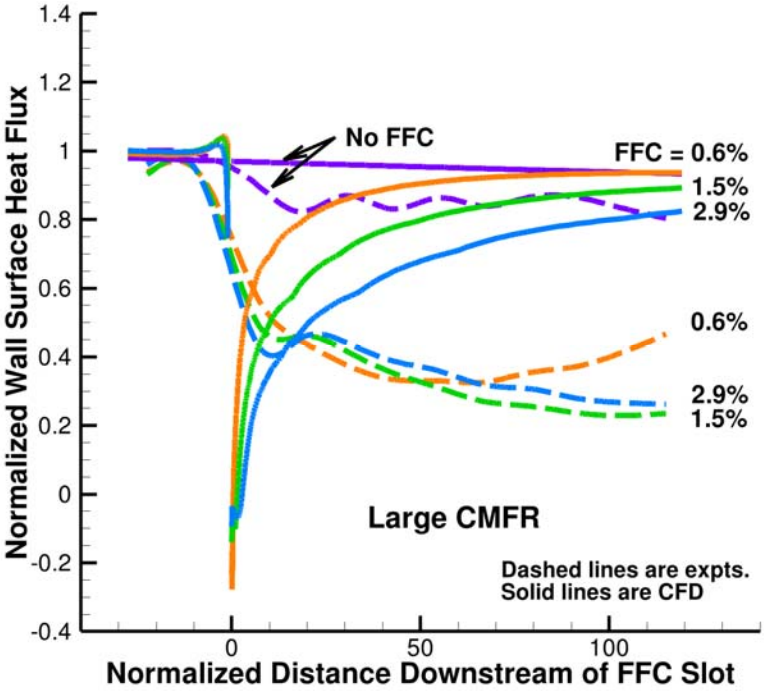

**Figure 11. Comparison of CFD with Experiment for large CMFR.**

Fig. 11 shows the CFD predictions of wall surface heat flux for multiple FFC flow rates, all with the large CMFR, compared with experimental data for the corresponding cases. The heat flux is taken as positive when heat is transferred from fluid to wall. The solid curves are CFD simulation results, while the dashed lines are experimental data. We see in the case when no FFC was present, shown in purple, that both CFD and experiment show a basically horizontal shape. This relatively constant behavior is to be expected, because the thermal boundary layer and the driving temperature difference are not changing very much. In the cases where FFC is present, both CFD and experiments show a reduction in the heat flux, although the level of heat flux reduction observed in the experiment is far larger than that predicted by CFD.

In the FFC=1.5% case, the experimental data (green dashed line) show a large film cooling effect downstream of the slot. However, one puzzling aspect of the experimental data is that the heat flux just downstream of the slot is not lower. It might be expected that the cool fuel issuing from the slot has not traveled far enough downstream to be heated enough by turbulent convection from the hot gas to produce the observed heat flux. Another puzzling aspect of the experimental data is that the film cooling effect increases with distance from the slot for about the first two-thirds of the cooled panel, i.e. the heat flux decreases. This increase in the cooling may be attributed to the increasing thickness of the layer of coke that is created on the wall surface, which acts as a thermal barrier. A further observation has to do with the effect of increasing the FFC flow rate. Just downstream of the slot, the experimental heat flux shows the expected dependence on the FFC flow rate, i.e., higher flow rates lead to more cooling. Further downstream, however, the experimental case with FFC=0.6% provides the most cooling, while still further downstream it again provides the least. Also, over most of the cooled wall region, FFC=2.9% provides less cooling than FFC=1.5%. Possibly, this experimentally observed behavior is due to the FFC=0.6% film heating up early and using up most of its soot capacity, while the FFC=2.9% stays cooler than the outer layer of the FFC=1.5% film and thus forms less soot. Thus, the inclusion of soot models is likely to be of significance for predicting these effects.

The CFD results appear to follow the expected trends without the inclusion of soot effects. The results show a decrease in heat flux just downstream of the slot, due to the cooling effect of the injected kerosene. Beyond that, the CFD cases show the heat flux increasing with distance downstream of the slot, as the film is heated up by the core flow. Moreover, the cooling predicted by CFD simulations scales positively with FFC flow rates in a manner consistent with the physics included in the model. In Fig. 12, we see much the same trends in the simulation results for multiple FFC flow rates with the small CMFR, as compared with experimental data. Again, the key differences in the predicted and measured results may be attributed to the absence of soot and coke deposition in the model.

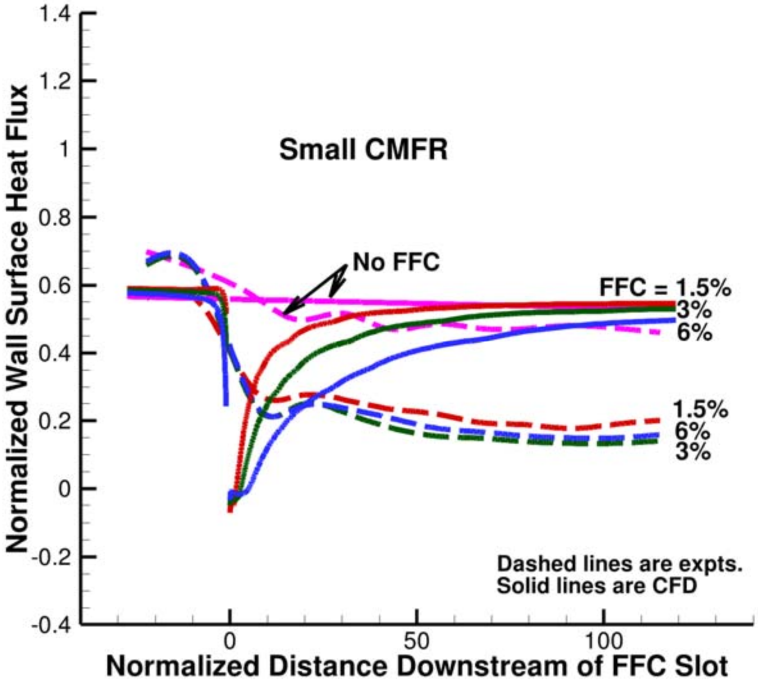

Figure 12. Comparison of CFD with Experiment for small CMFR.

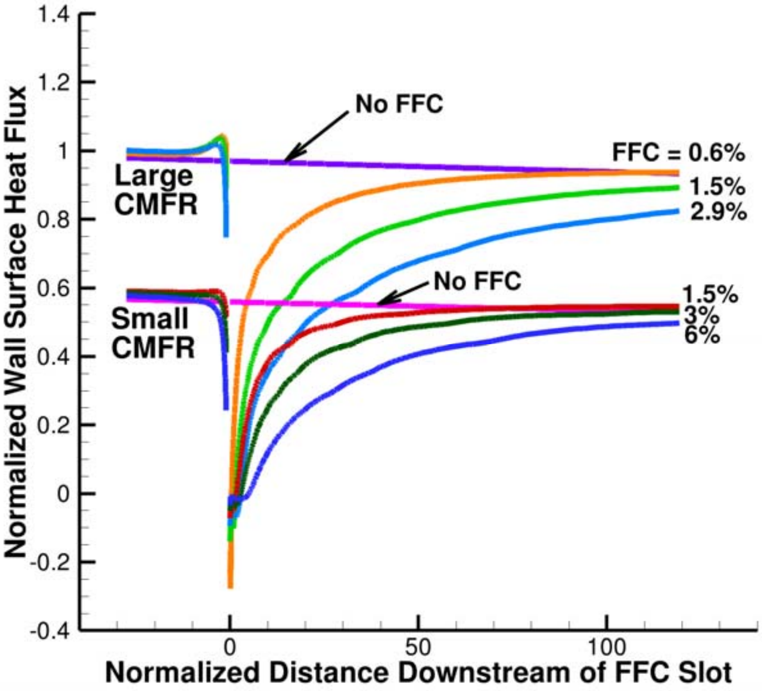

Figure 13. Sensitivity of Wall Heat Flux to CMFR and FFC flow rate.

The simulation results of the previous two figures are re-plotted in Fig. 13, for convenient comparison with each other. The large CMFR cases have a larger core gas speed than the small CMFR cases. It is seen from the figure that the model shows the expected increase in convective heat flux with increase in core gas speed.

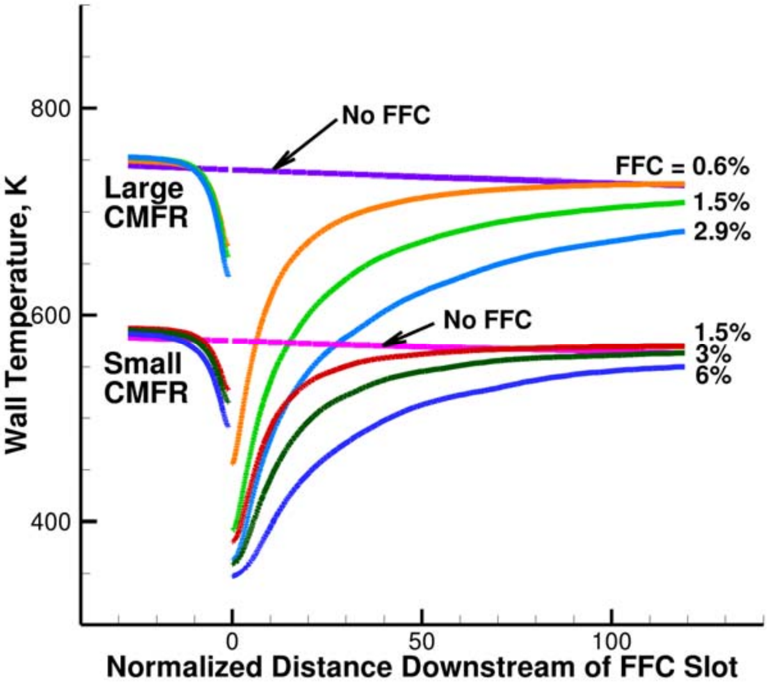

**Figure 14.Sensitivity of Wall Surface Temperature to CMFR and FFC flow rate.**

Fig. 14 shows the predicted wall surface temperature for the six cases involving the two CMFRs. Not unexpectedly, the curves have the same shapes as the heat fluxes in Fig. 13. This follows from the wall thickness, convective heat transfer coefficient and cooling water temperature being assumed the same for all cases. Furthermore, the wall surface temperatures are all in the reasonable range, which again follows from the fact that the cooling system was designed to safely remove the observed heat flux levels.

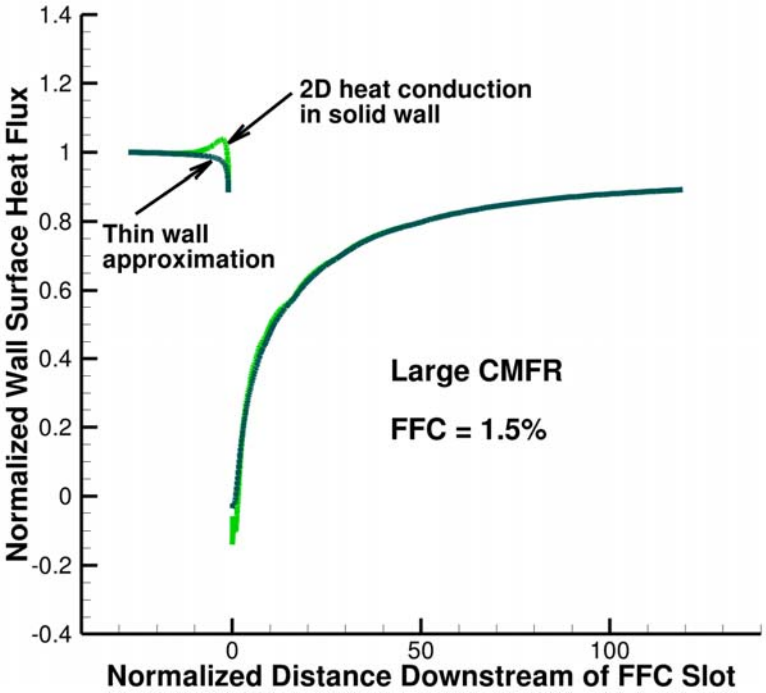

**Figure 15. Thin wall versus full conjugate heat transfer.**

Fig. 15 is a comparison between the baseline case with the full conjugate heat transfer calculation involving two-dimensional heat conduction in the wall, and a simplified simulation wherein the 2-D heat conduction is replaced with a thin-wall approximation. In the latter, the heat conduction is assumed to be purely one-dimensional, taking place in a direction transverse to the wall. The simplification saves a little computational effort, and does not need the generation of a mesh in the solid wall or even the representation of the wall geometry other than the specification of just a wall thickness and wall material. It is seen that except for small departures in the vicinity of the FFC slot, the simplified model predicts heat fluxes almost identical to those predicted by the full model. This indicates that in the cases considered in this paper, given the simplified representation of the cooling water channels, heat conduction along the wall does not play a large role. It further indicates that heat conduction along the wall does not account for the feature of the experimental data in Figs. 11 and 12 that the wall heat flux immediately downstream of the FFC slot is of approximately the same level as the heat flux further downstream. In the simulation results, the heat flux just downstream of the slot is considerably lower than it is further downstream.

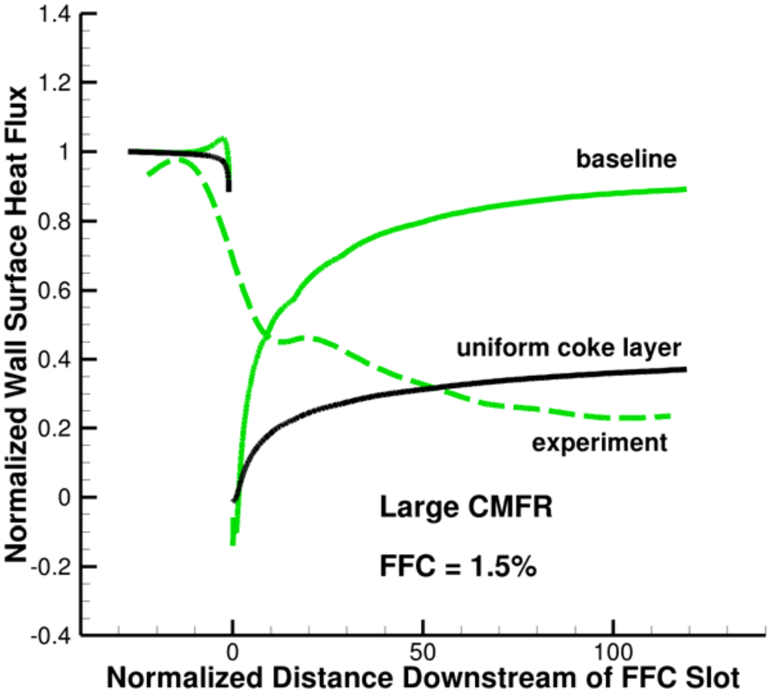

**Figure 16. Sensitivity of wall heat flux to carbon layer on wall.**

Although we do not have a detailed soot and coking model in our calculations, we carried out calculations by replacing the copper wall with a thin coke layer. The thermal conductivity of coke deposits varies depending on the type of deposit. Morris and Faircloth[8] give estimates of the thermal conductivity of petroleum coke (fuels) as ranging from 0.4 W/m-K to 2 W/m-K. The value of 1 W/m-K was selected as being representative. The model was solved with various coke layer thicknesses until the desired level of heat flux reduction was obtained. Fig. 16 shows the results for the wall heat flux. The coke layer thickness corresponding to this heat flux level is 65 micrometers, which is a plausible number that falls within the range of observed carbon deposit thicknesses in hydrocarbon pyrolysis phenomena. If carbon deposition is the cause of the experimentally observed large heat flux reduction seen in Fig. 16, then the carbon layer would not be of uniform thickness as in our simulation, but must increase in thickness downstream. This increasing thickness would also need to offset the rising temperature of the fuel film in order to show the downward trend seen in the figure before it finally flattens out.

Fig. 17 shows the surface temperatures corresponding to Fig. 16. As expected, the metal surface temperature is greatly reduced by the insulation of the coke layer, as compared with the baseline case. Interestingly, the surface of the coke layer exposed to the fuel film is predicted to get quite hot.

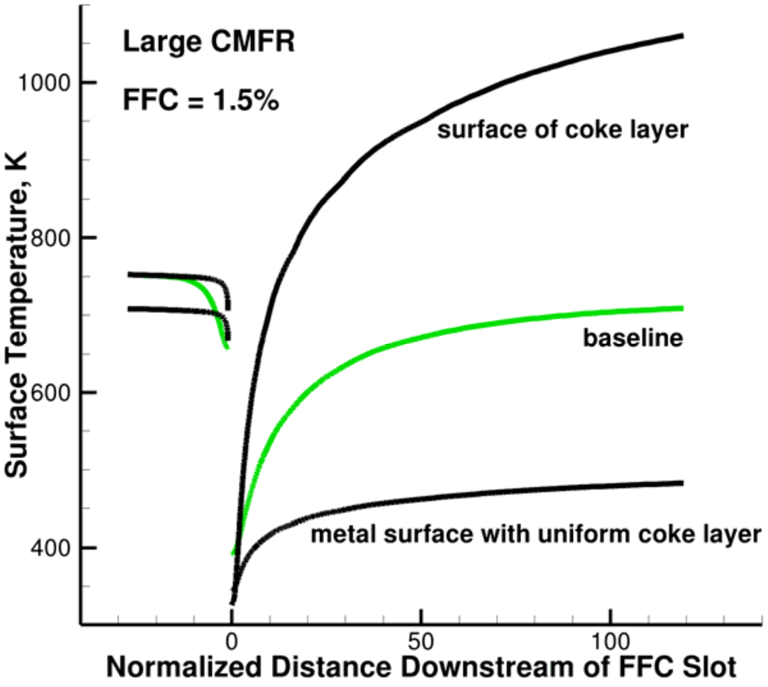

**Figure 17. Sensitivity of surface temperature to carbon layer on wall.**

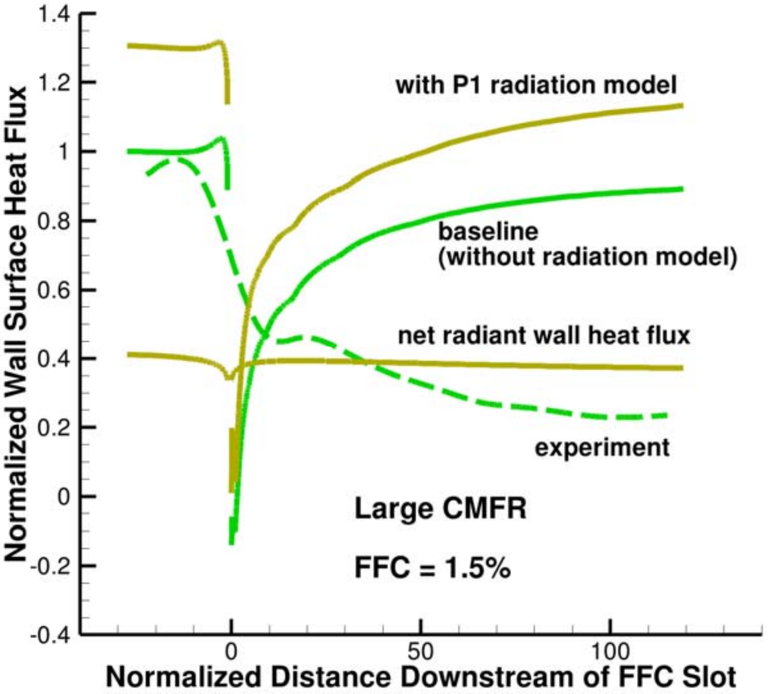

**Figure 18. Sensitivity of wall heat flux to radiation.**

Next, we examined the sensitivity of the heat flux to radiative heat transfer. For the baseline case, we included the P1 model available in Fluent. This augments the CFD model by solving the radiative transfer equation in a participating medium. We assumed that the fluid mixture is a gray medium, wherein the absorption coefficient is independent of the wavelength of the radiation. An absorption coefficient of 40 per meter was used. The wall was treated as a black body radiator. The results are shown in Fig. 18. We see that the predicted radiant wall heat flux is of the same order of magnitude as the predicted convective heat flux. Therefore, a key finding is that under the conditions of the laboratory experiments, thermal radiation plays a sizable role, and must be accounted for in the mathematical model.

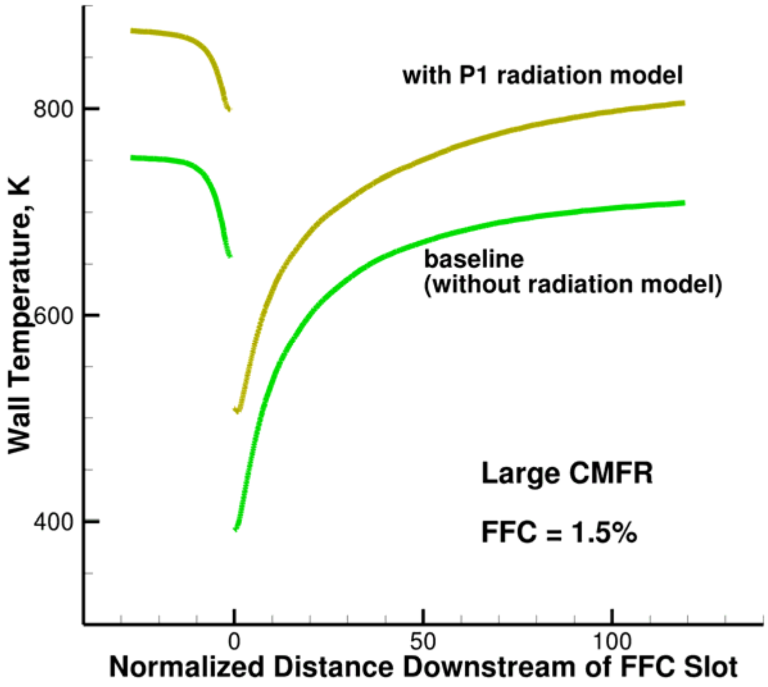

**Figure 19. Dependence of wall temperature on radiation.**

Fig. 19 shows the predicted wall surface temperatures for the cases of Fig. 18. It is seen that radiation can produce a significant rise in the wall surface temperature, which in turn leads to a decrease in the convective heat flux as compared with the baseline case. This explains why the total heat flux with radiation in Fig. 18 is not the sum of the baseline (convective) heat flux and the net radiant heat flux that are shown in that figure.

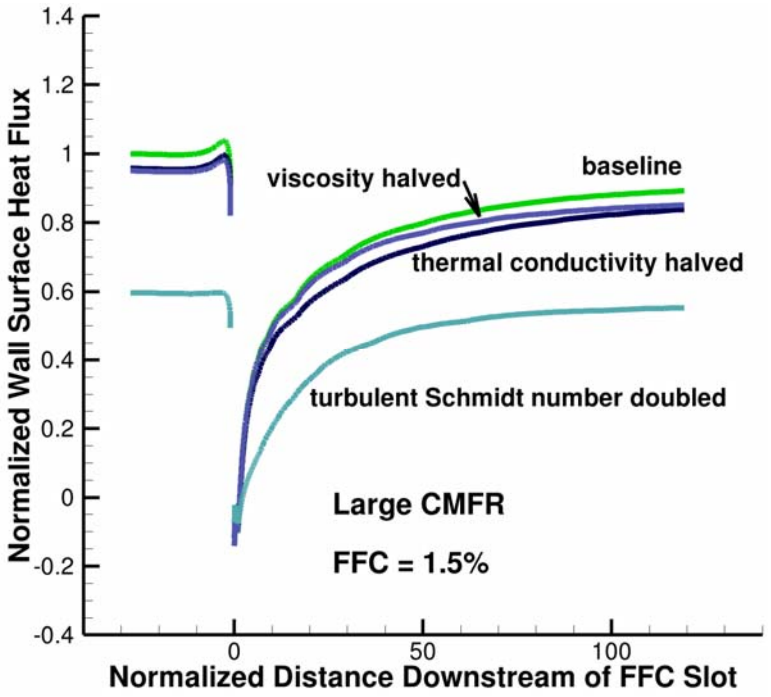

**Figure 20. Sensitivity of wall surface heat flux to transport properties.**

Next, the sensitivity of the wall surface heat flux to transport property values was examined. The assumed values of the coefficient of viscosity, thermal conductivity and turbulent Schmidt number were perturbed in independent tests. The results are shown in Fig. 20. It is seen that halving the coefficient of molecular viscosity did not change the predicted wall heat flux dramatically. Halving the molecular thermal conductivity had a somewhat bigger effect, but this was also not large enough to account for the experimentally observed levels. It is likely that varying the mass diffusivity would have a similar minimal effect. Variation of the turbulent mass diffusivity, however, leads to a more significant change. The turbulent Schmidt number, which is the ratio of the turbulent momentum diffusivity and the turbulent mass diffusivity, was doubled from its default value of 0.85. Because the turbulent momentum diffusivity is determined by the turbulence model, in effect this doubling halves the turbulent mass diffusivity. This resulted in a dramatic lowering of the heat flux both upstream and downstream of the FFC slot. The turbulent mass diffusivity controls the mixing rate between the fuel film and the core flow. It is plausible that the turbulent binary mass diffusivity of supercritical fluids of large density ratio is significantly lower than for ideal gases at atmospheric conditions. This sensitivity evaluation identified the turbulent mass diffusivity as needing to be more accurately characterized in the model.

## V. Summary and Conclusions

A model was constructed for the numerical simulation of heat transfer to and within walls that are cooled by injection of a cool fluid through a wall slot. The fluid physics model comprises a steady-state, compressible flow model with convective, radiative and conjugate heat transfer, with a RANS turbulence model, with equilibrium chemistry in a conserved mixture-fraction formulation. We attempted to validate the model with experimental wall heat-flux data. Simplifying approximations and omissions made while constructing the fluid model and the model of the experimental arrangement were listed and discussed.

The CFD simulations predicted flow fields and wall surface heat transfer that display trends expected from the physics model used in this study, for example trends with respect to changes in CMFR and FFC flow rate. They provide predictions that are in reasonable agreement with experimental values when fuel film cooling is not present. The current model is a first step towards reliable and accurate prediction of fuel film cooling effectiveness. The wall heat flux predictions obtained from the current model are of the same order of magnitude as the experimental measurements when FFC is present. However, the CFD predictions are not in full agreement with the values or trends of the experimental data when fuel film cooling is present. The model is missing some important physics, and consequently it does not provide insight into non-classical scaling behavior of the heat flux as observed in experiment

We performed sensitivity studies of the wall heat flux with respect to model parameters and assumptions. Based on these studies, the key factors influencing wall heat flux were identified. A key finding of the current study is that thermal radiative heat transfer is significant under the conditions of the experiment. It must therefore be included in the model in order to predict the level of heat flux found in the experimental data. The other key factors that were identified are the deposit of a thermally insulating carbon layer on the film-cooled wall, and the appropriate function to be used for the turbulent mass diffusivity of kerosene mixing with lighter species under supercritical conditions.

## VI. Future Work

The weaknesses of the current model provide the directions for future efforts to improve the model and use it to optimize the FFC technology. In further model improvements, thermal radiation must be an integral part of the model, with realistic estimates of mean absorptivity and emissivity of a soot-heavy dense fluid. The turbulent mass diffusivity of supercritical mixtures must be considered and a more accurate model must be developed. The next step toward more accurate thermochemistry will be to include moderately non-equilibrium pyrolysis chemistry via a flamelet model. This may further allow the incorporation of soot formation and oxidation within the conserved-scalar/flamelet formulation. The model will then be extended to include coke deposition on wall and the associated thermal barrier effect. The sooting and coking may require a switch to the more expensive finite-rate chemistry formulation. Another topic of future study is the interaction between successive FFC slots and its impact on optimal slot placement.

## References

[1] Yang, W., and Sun, B., “Numerical Simulation of Liquid Film in a Liquid Oxygen/Rocket Propellant 1 Liquid Rocket”, *Journal of Thermophysics and Heat Transfer*, Vol. 26, No. 2, April-June 2012.

[2] Wang, T.-S., “Thermophysics Characterization of Kerosene Combustion,” *Journal of Thermophysics and Heat Transfer*, Vol. 15, No. 2, 2001, pp. 140–147.

[3] Kirchberger, C., Schlieben, G., and Haidn, O.J., “Assessment of Analytical Models for Film Cooling in a Hydrocarbon/ GOX Rocket Combustion Chamber”, AIAA 2012-3909, 48th AIAA/ASME/SAE/ASEE Joint Propulsion Conference & Exhibit, Atlanta, GA, July 2012.

[4] McBride, B.J., *CEA – Chemical Equilibrium with Applications* [online database], URL: http://www.grc.nasa.gov/WWW/CEAWeb/ [cited March 2013].

[5] Modest, M.F., *Radiative Heat Transfer*, 3rd ed., Academic Press, Amsterdam, the Netherlands, 2013.

[6] Menter, F.R., “Two-Equation Eddy-Viscosity Turbulence Models for Engineering Applications”, *AIAA Journal*, Vol. 32, No. 8, 1994, pp. 1598-1605.

[7] Peters, N., *Turbulent Combustion*, Cambridge University Press, Cambridge, U.K., 2000.

[8] Morris, E. G., and Faircloth, J.M., “Thermal and Electrical Properties of Petroleum Cokes,” *13th Biennial Conference on Carbon*, American Carbon Society, Aerospace Corp. and TRW Inc., 1977, pp. 214-215.

# Modeling of Fuel Film Cooling on Chamber Hot Wall

**Presented at:**

***50th Joint Propulsion Conference, 28–30 July 2014, Cleveland, OH***

**Ananda Himansu, Edward B. Coy,**
**Venkateswaran Sankaran, Steven A. Danczyk**
**Air Force Research Laboratory**

*Integrity ★ Service ★ Excellence*

# Outline

- Goals of M&S of fuel film cooling (FFC)
- Physics and chemistry of FFC for hydrocarbon liquid rocket engines (LRE)
- Previous research
- Physics/chemistry models and approximations
- Validation cases
- Sensitivity studies
- Summary and Conclusions
- Planned research

# M&S Goals for Fuel Film Cooling Technology Advancement

- Provide LRE designers with predictive physics-based numerical simulation tools for Fuel Film Cooling (FFC) to enable design optimization
- Use best available physics and chemistry models, evaluate strengths and weaknesses
- Accuracy of available M&S tools estimated by validation against lab-scale experimental data of known uncertainty
- Perform sensitivity studies to identify and rank influential variables
- Refine the models as needed
- Help design improved lab validation experiments
- Current study is an initial step

# Physics and chemistry of fuel film cooling

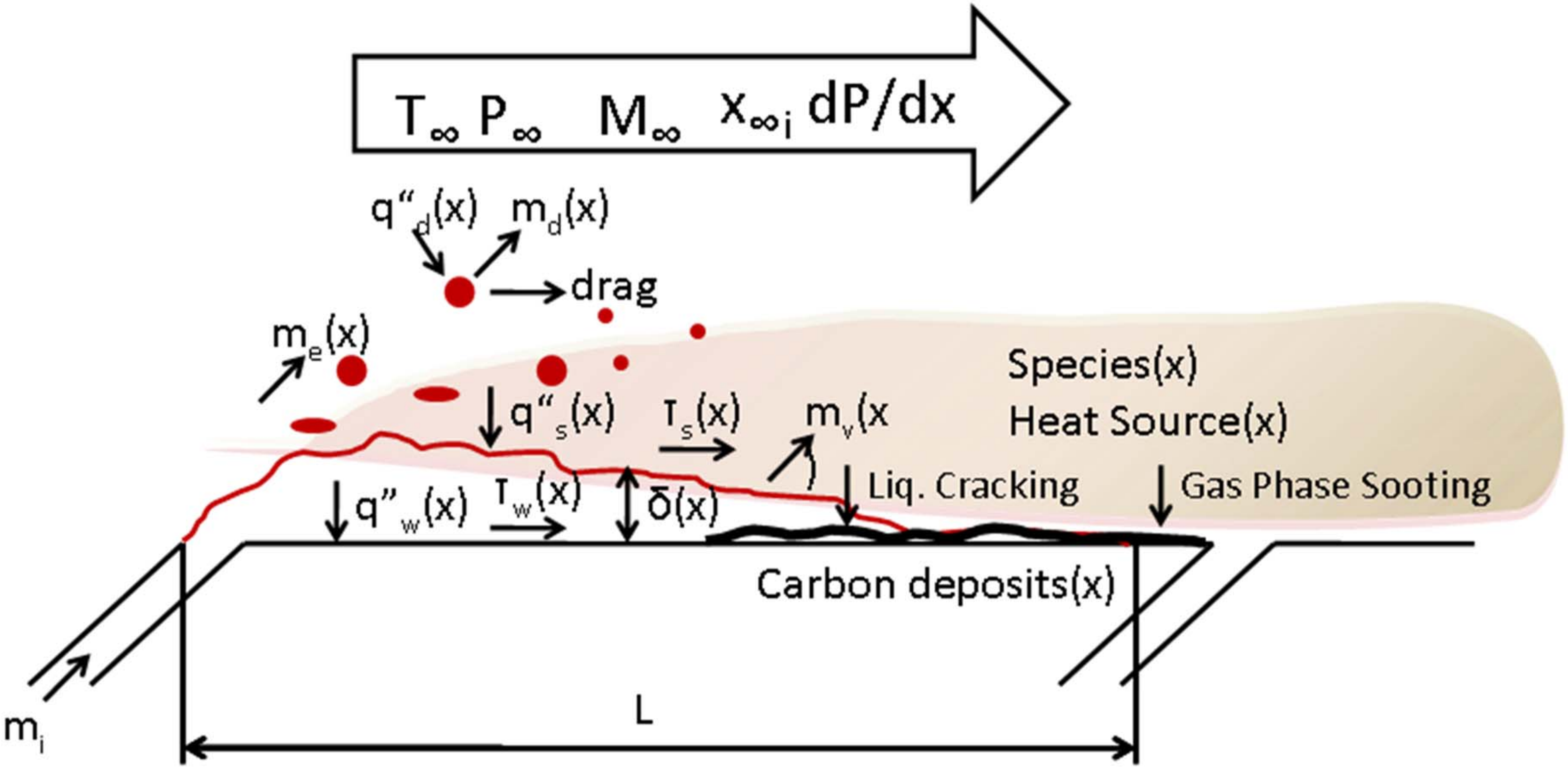
$T_\infty$ $P_\infty$ $M_\infty$ $X_{\infty i}$ dP/dx
$q"_d(x)$ $m_d(x)$
drag
$m_e(x)$
Species(x)
Heat Source(x)
$q"_s(x)$
$T_s(x)$
$m_v(x$
$q"_w(x)$
$T_w(x)$
$\delta(x)$
Liq. Cracking
Gas Phase Sooting
Carbon deposits(x)
L
$m_i$

# Challenging Physics and Chemistry

- Turbulent reacting flow with large heat transfer rates
- Supercritical pressure and high density ratio implies some uncertainty in turbulent transport properties
- Large temperature range causes large variations in fluid properties, reaction rates and composition
- Cool kerosene jet in hot cross-flow; jet partially entrained, rest forms wall film protecting wall
- Film is heated and pyrolyzed (endothermic reaction)
- Soot is formed, partially oxidized; transported soot forms protective thermal barrier deposits on wall
- Radiative and conjugate heat transfer (CHT) present

# Previous M&S of kerosene FFC

- Yang and Sun (2012) modeled kerosene FFC, used finite-rate kerosene combustion chemistry model
  - Parametric study, no comparison with experimental data
- Kirchberger, Schlieben and Haidn (2012) used analytical and semi-empirical film-cooling models
  - Comparison with experiment deemed unsatisfactory

# Current Numerical Model

- Start with simpler model; evaluate accuracy, and refine models as needed
- 2-D steady-state mean flow; Navier-Stokes equations with conjugate heat transfer (coupled convection in the fluid and conduction in the solid); P1 radiation model
- RANS turbulence model, SST k-ω with solve-to-wall
- Ideal-gas mixture with kerosene vapor; constant laminar transport properties of mixture at 800K from CEA
- Conserved scalar approach: tracks mean mixture fraction and its variance, and the mean enthalpy (advantage: fewer equations and no chemistry source terms)
- Equilibrium chemistry (mixed is reacted)
- CFD software used: ANSYS Fluent 15

# Validation Cases

- Experimental wall heat flux data from lab-scale tests
- Square cross-section test article, FFC panel as one wall
- Nominal pressure 700 psi
- Nominal oxygen/kerosene mixture ratio 2.8
- Two Core Mass Flow Rates (CMFRs): Small and Large
- Small CMFR: FFC rates of 0, 1.5%, 3% and 6%
- Large CMFR: FFC mass flow rates of 0, 0.6%, 1.5%, 2.9%

# Boundary Conditions and Model Parameters

- Hot gases at inlet; composition and temperature (3680K) from CEA; small or large CMFR
- FFC mass flow rates from expt.; inlet temperature 305K
- Symmetry BC at far wall; boundary layer neglected
- Material of all walls is copper
- Water cooling embedded in walls modeled by constant wall thickness with convective heat transfer BC
  - Constant convective heat transfer coefficient; constant “free-stream” water temperature of 350K
- Mixture thermal conductivity of 0.07383 W/m-K; viscosity $3.79 \times 10^{-5}$ Pa-s; absorption coefficient 40 /m
- Rich Flammability Limit set at default of 0.1
- Mesh of about 173,000 quadrilateral cells; wall y+ < 1

# Flow features: Film and Cooling Effect

**Cooling effect of film on wall immediately after slot, and on core flow near wall**

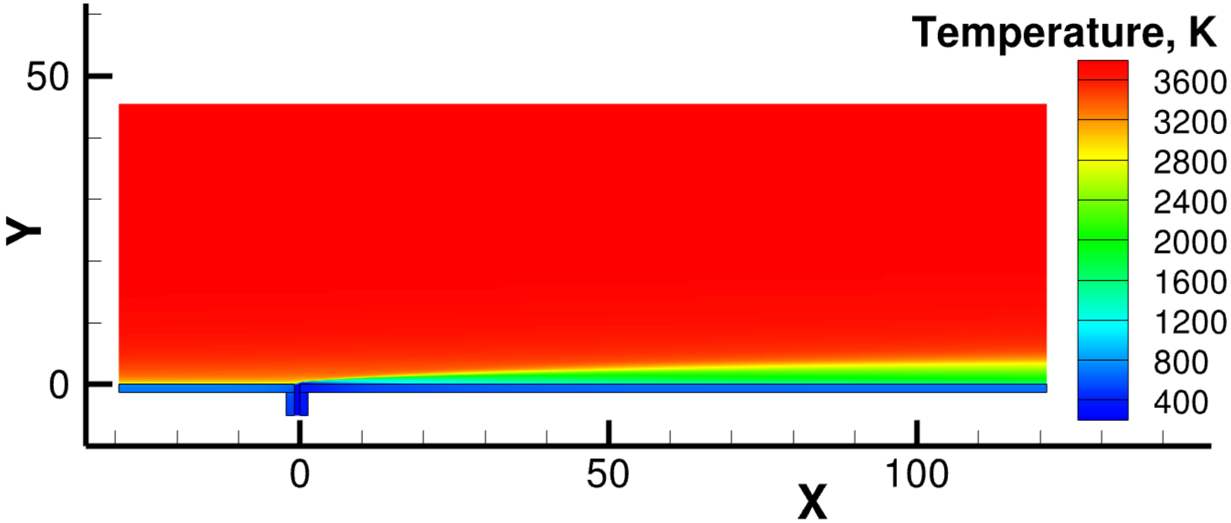

**Persistence of kerosene/products and diffusion between core and film**

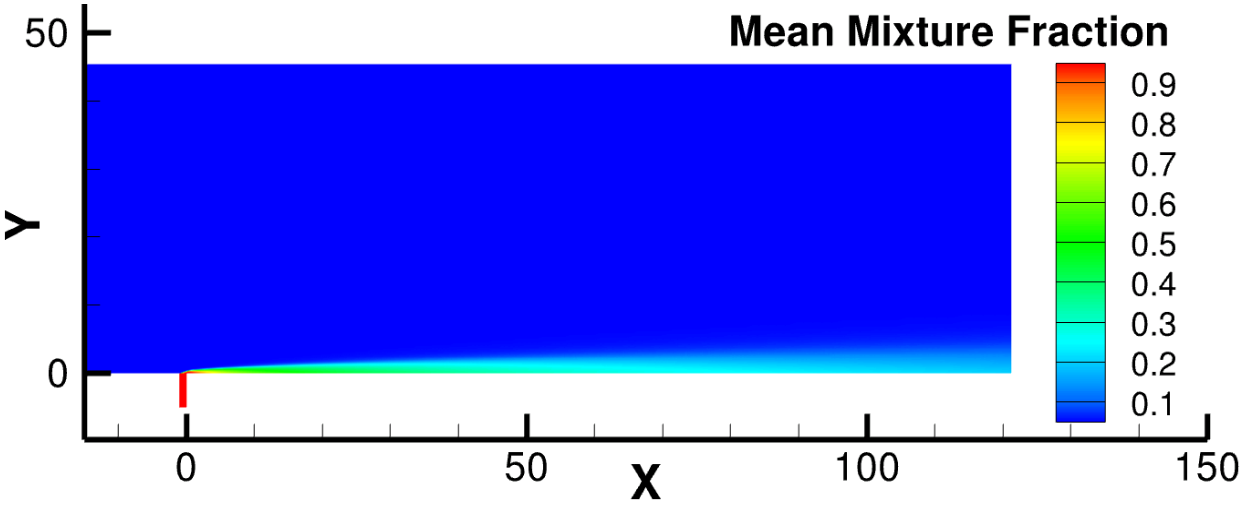

# Flow features: Chemistry

**Equilibrium chemical "pyrolysis" and "oxidation" of kerosene, controlled by temperature and diffusion between core and film**

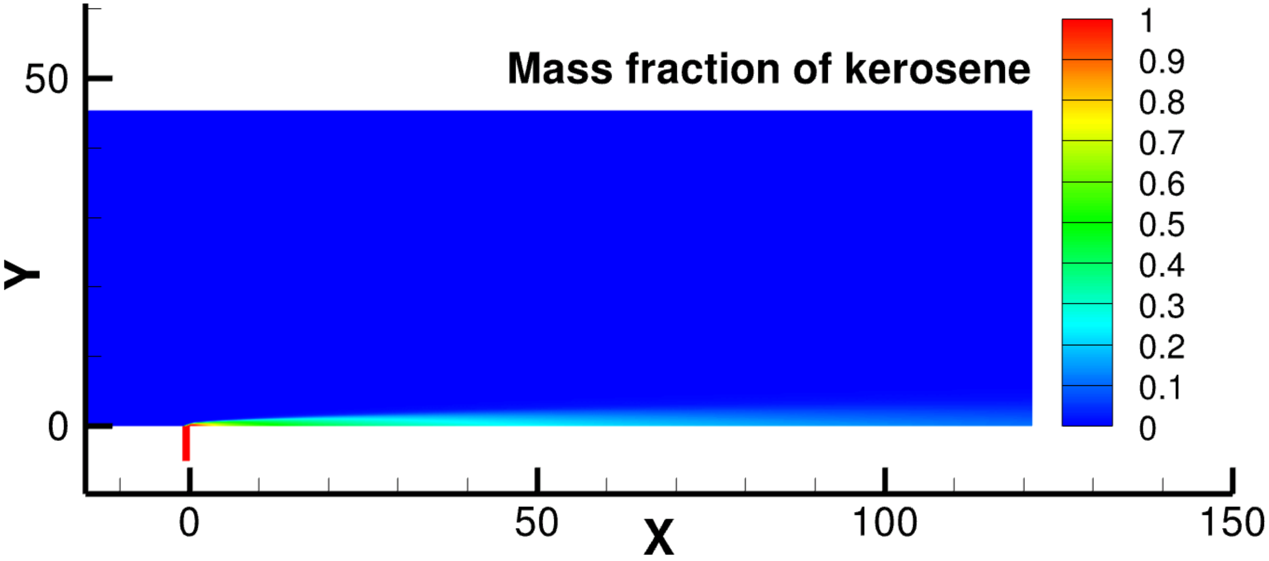

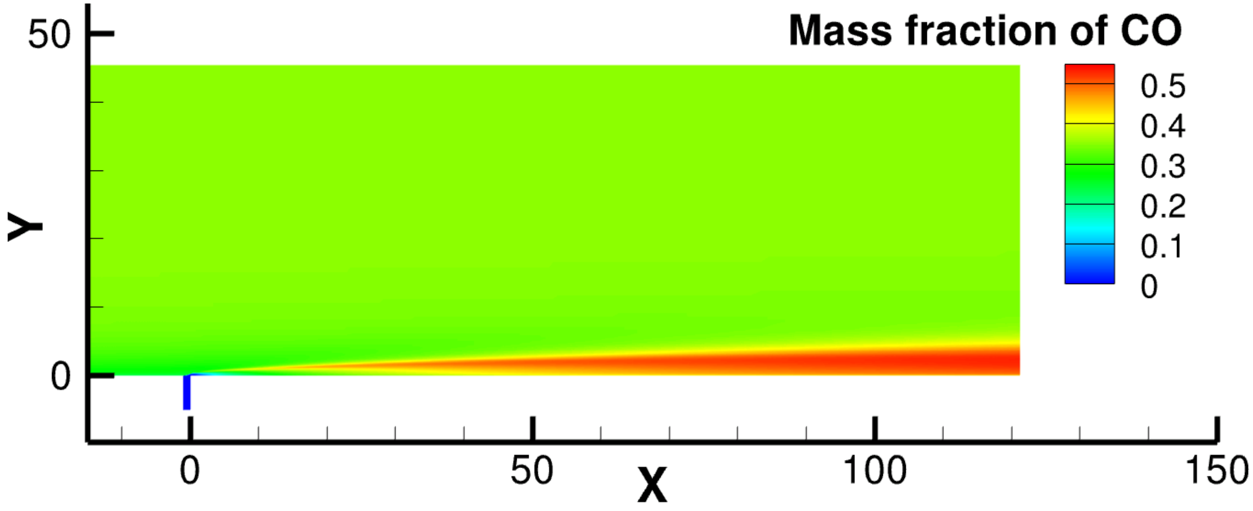

# Flow features: Shear layer

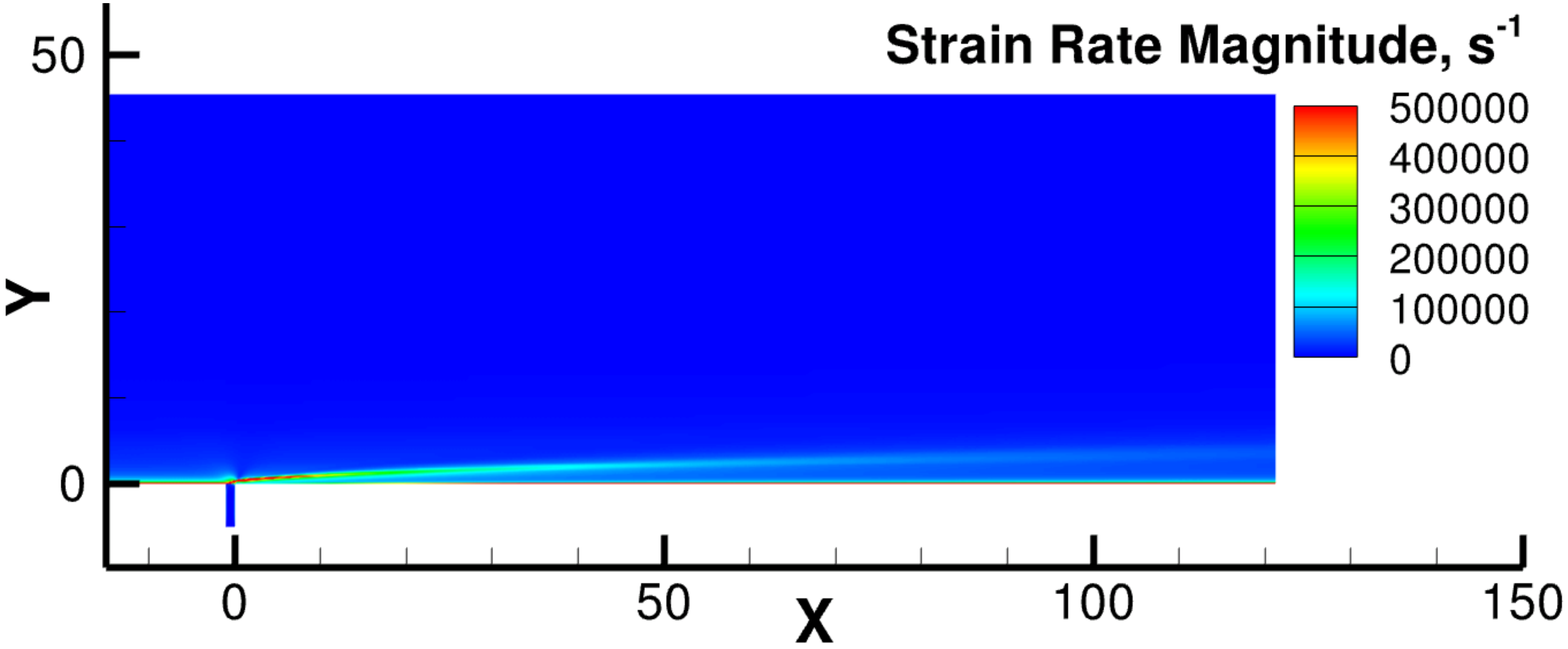

**Strong shear layer between core and film affects turbulent heat and mass transfer**

# Flow features: solution near FFC slot

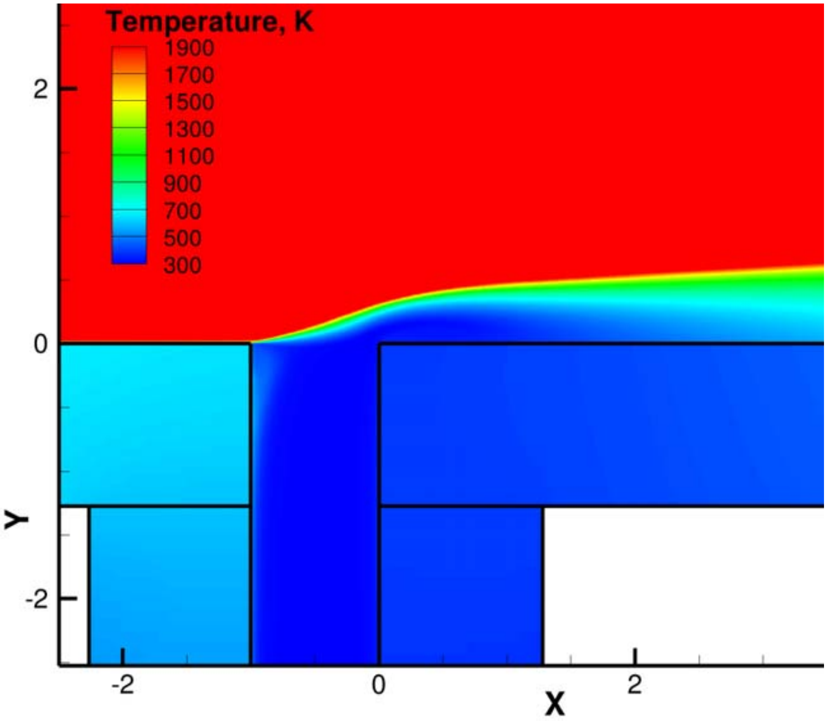

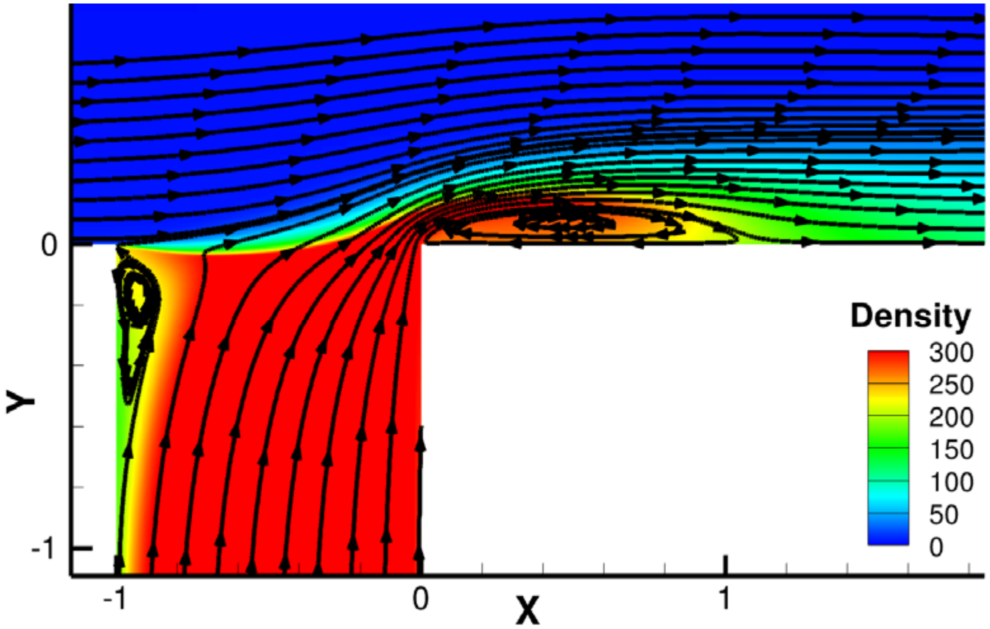

**Wall just after FFC slot cooler than wall upstream**

**High density kerosene jet; two recirculation regions**

# Selection of *h* for water cooling

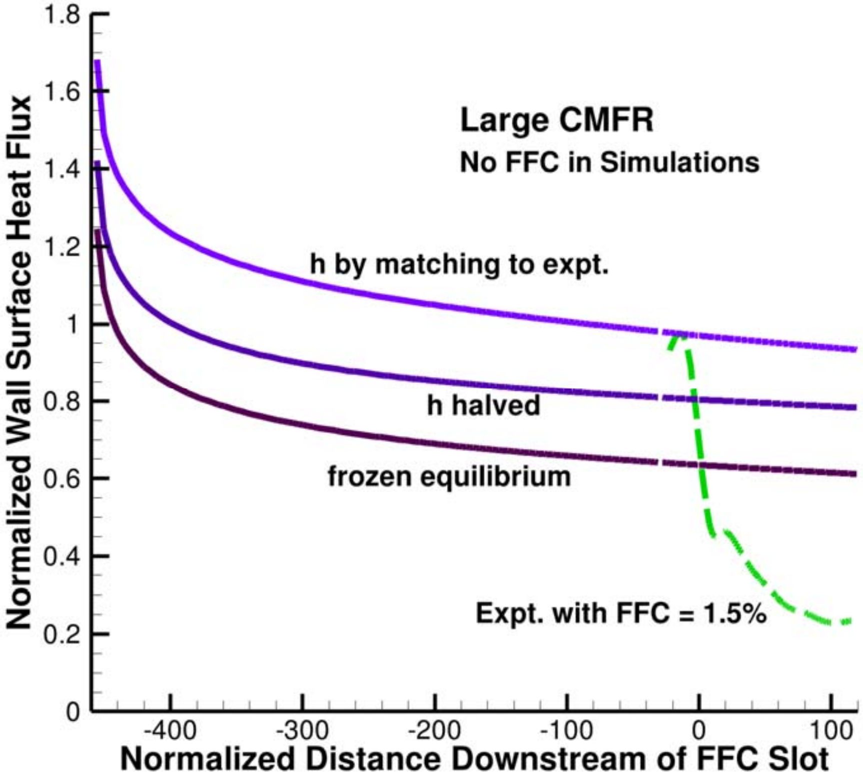

**Convective heat transfer coefficient for in-wall water cooling was selected so simulation matches experiment at start of test panel**

**Full chemical equilibrium needed from inlet onwards; frozen equilibrium at inlets greatly reduces heat transfer**

# Validation: Large CMFR

**Simulations display larger heat flux reduction by FFC just after slot than does expt.**

**Simulations display much smaller heat flux reduction elsewhere, than experiment**

**In simulations, best cooling occurs for largest FFC rate; in experiment, for medium**

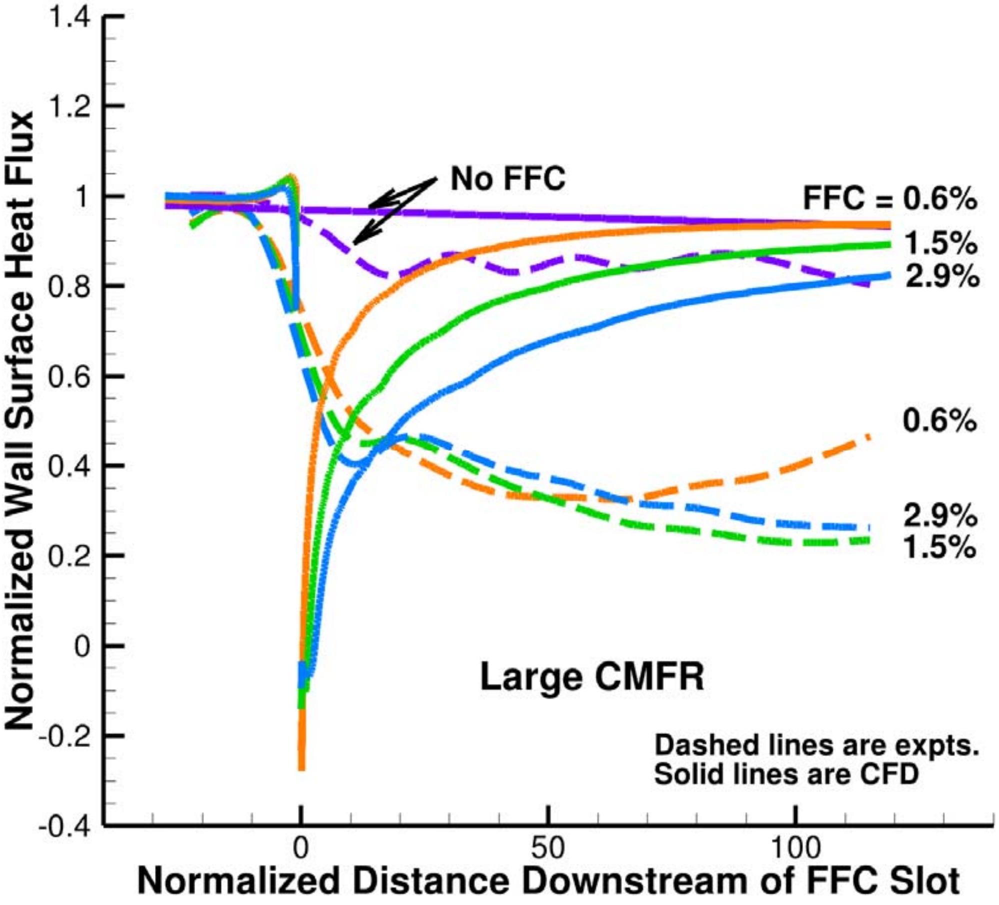

# Validation: Small CMFR

**For small CMFR, similar trends and discrepancies between simulations and expt.**

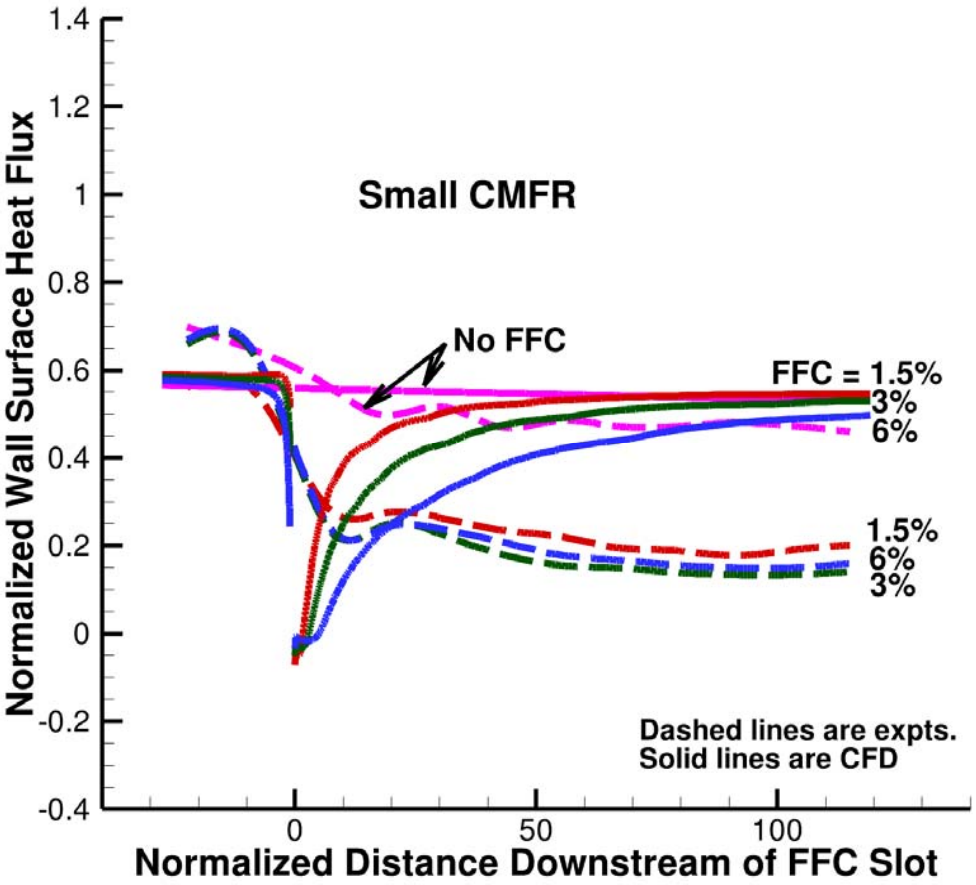

# Sensitivity to CMFR and FFC

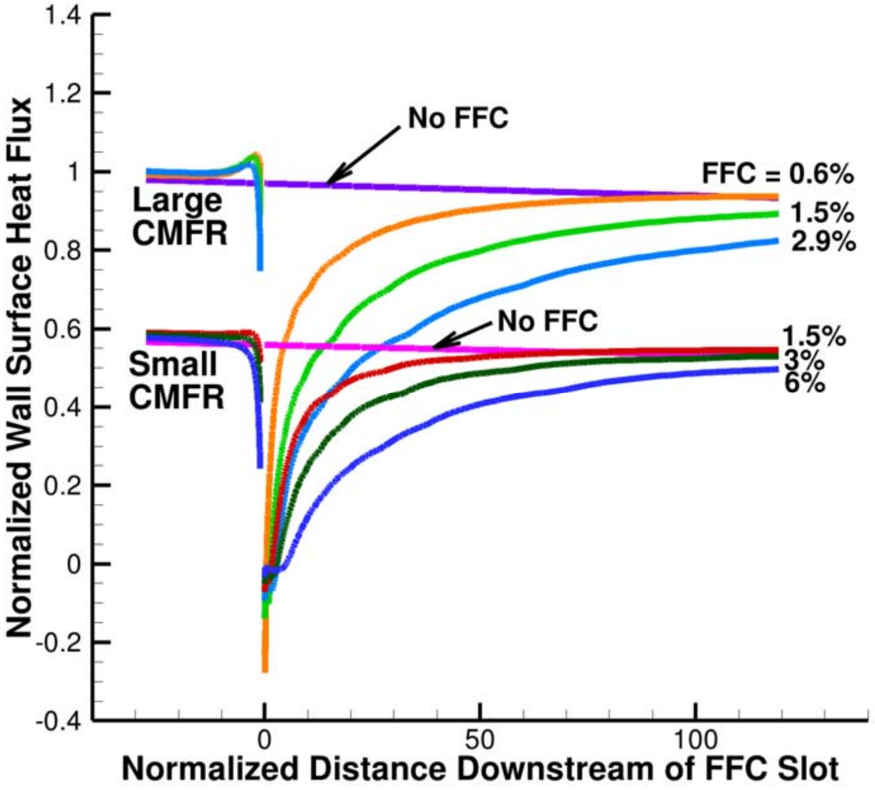

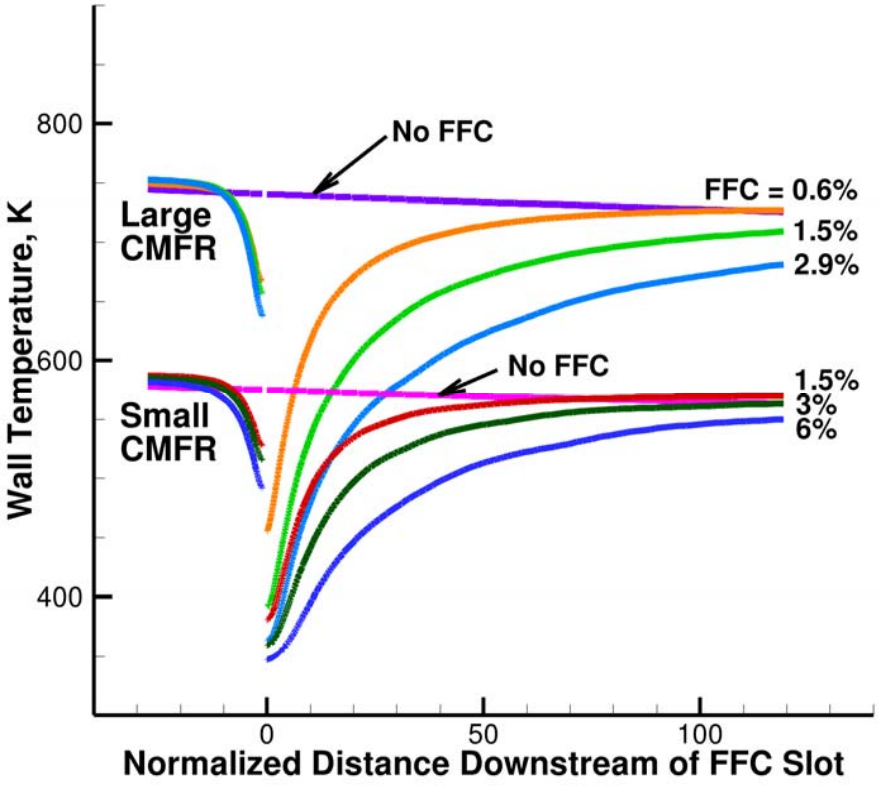

**Wall heat flux in simulations shows expected variations with changes in CMFR and FFC flow rates**

**Wall surface temperatures mirror heat fluxes**

# Thin-wall CHT approximation

"Thin-wall" approximation (one-dimensional heat conduction normal to wall surface in solid) is quite good, except in immediate vicinity of FFC slot

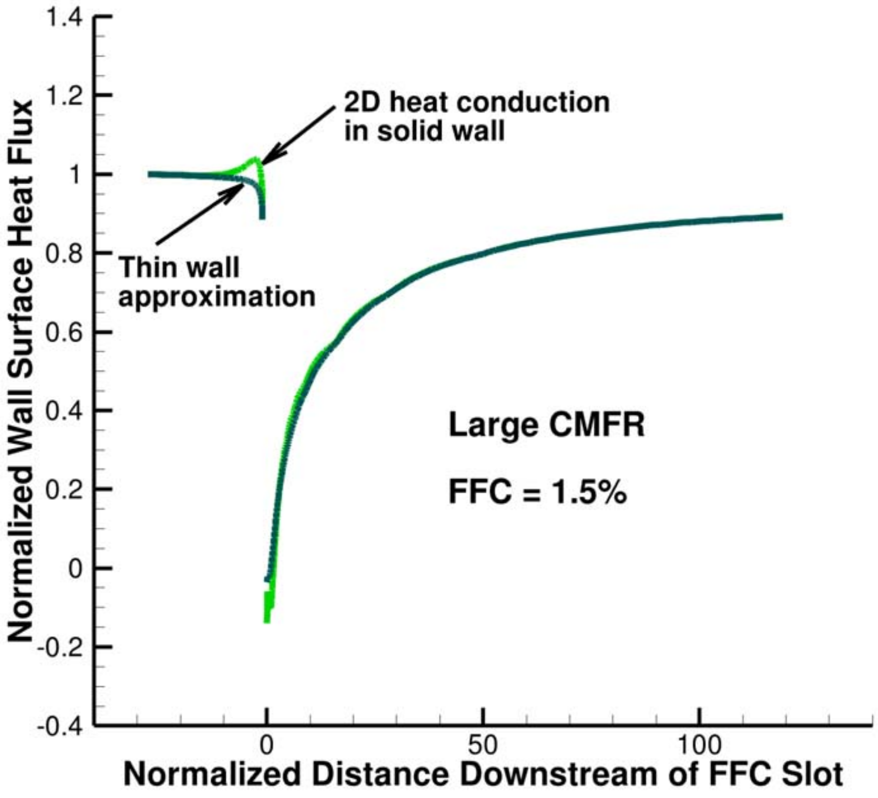

# Sensitivity to coke layer

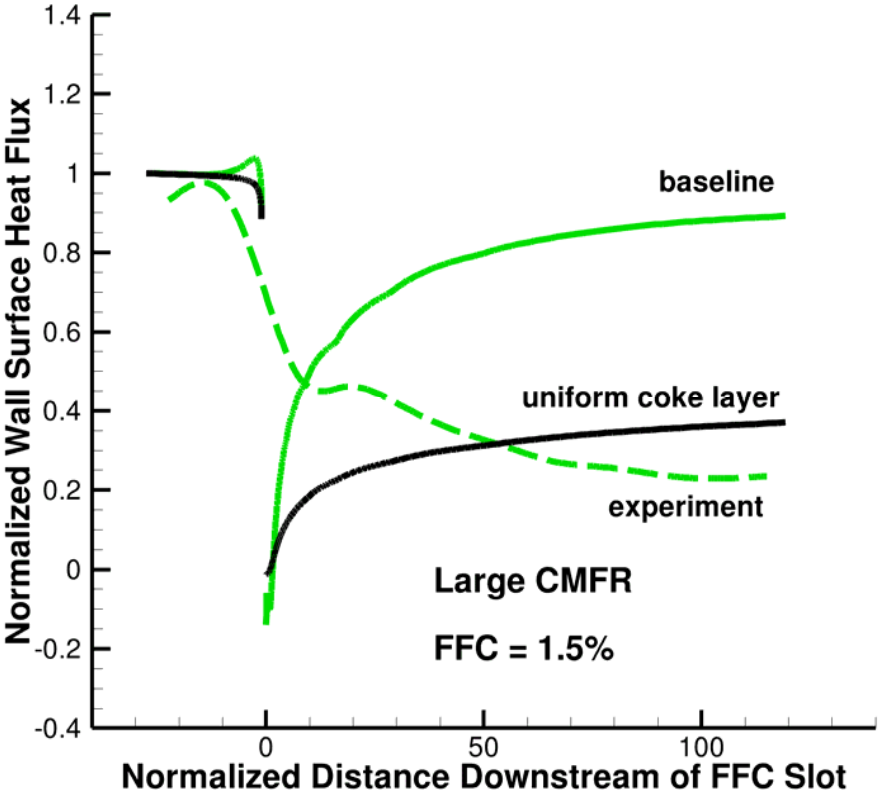

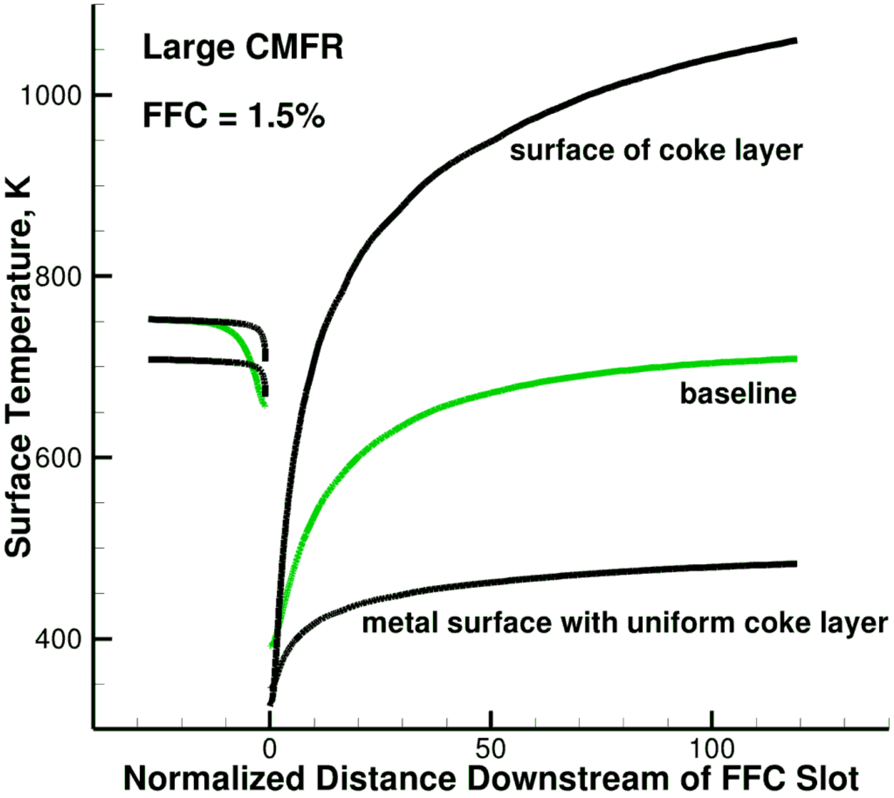

Simulated wall surface coke layer of uniform thickness with thermal conductivity of 1 W/m-K (Morris & Faircloth, 1977)

To match average heat flux reduction in experiment, simulated coke layer requires a thickness of 65 micrometers

# Sensitivity to Thermal Radiation

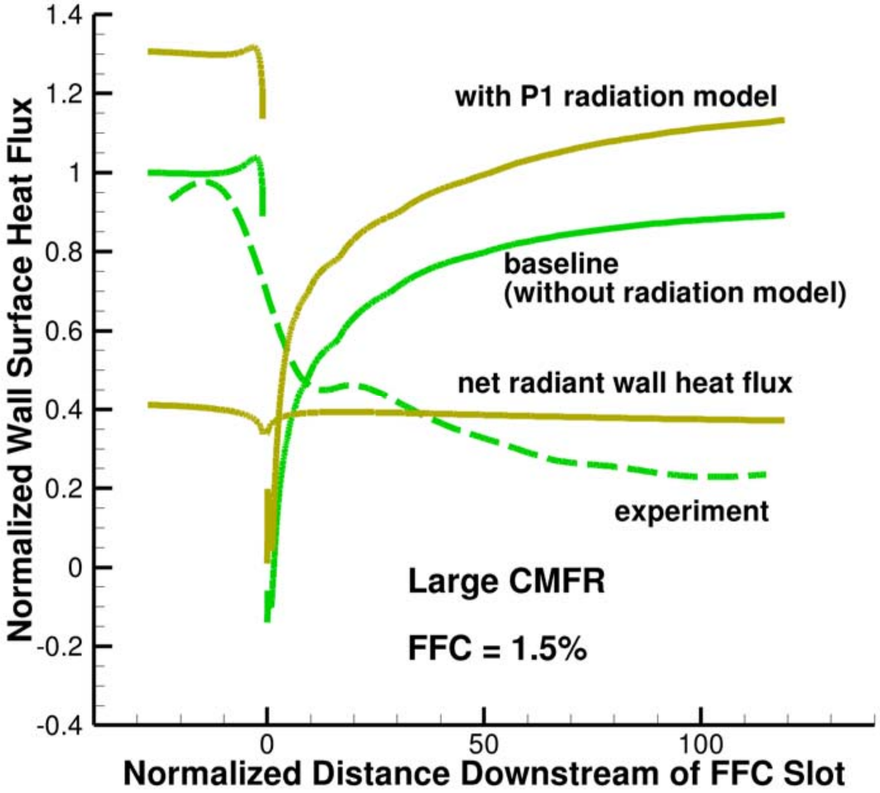

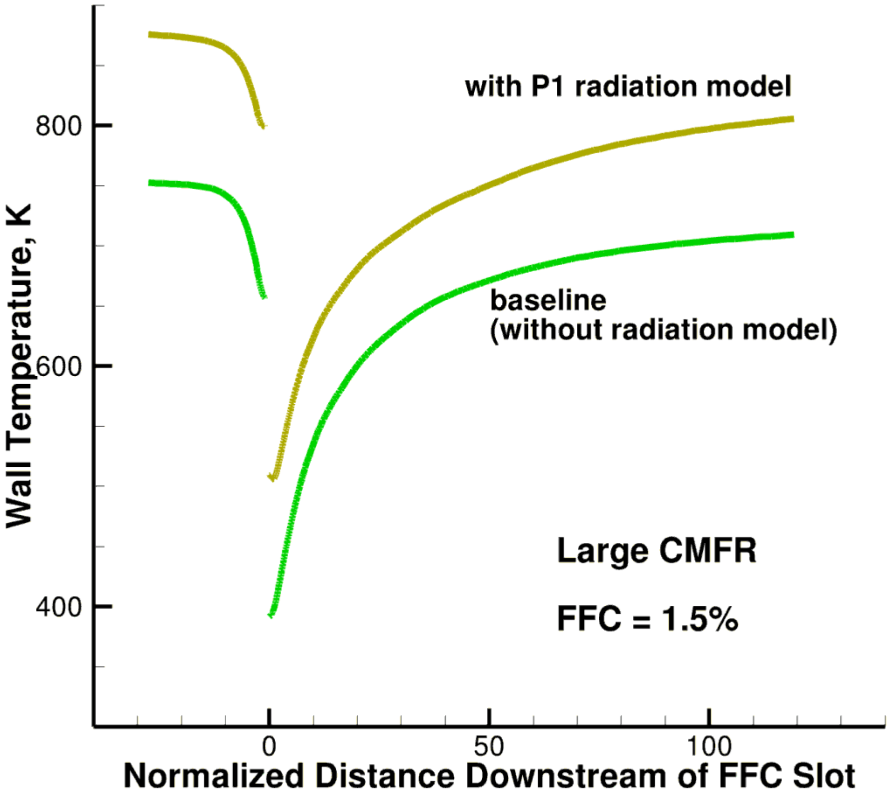

**Radiative wall heat flux predicted to be comparable to convective wall heat flux**

**Radiation lowers convective flux by raising wall surface temperature**

# Sensitivity to Fluid Properties

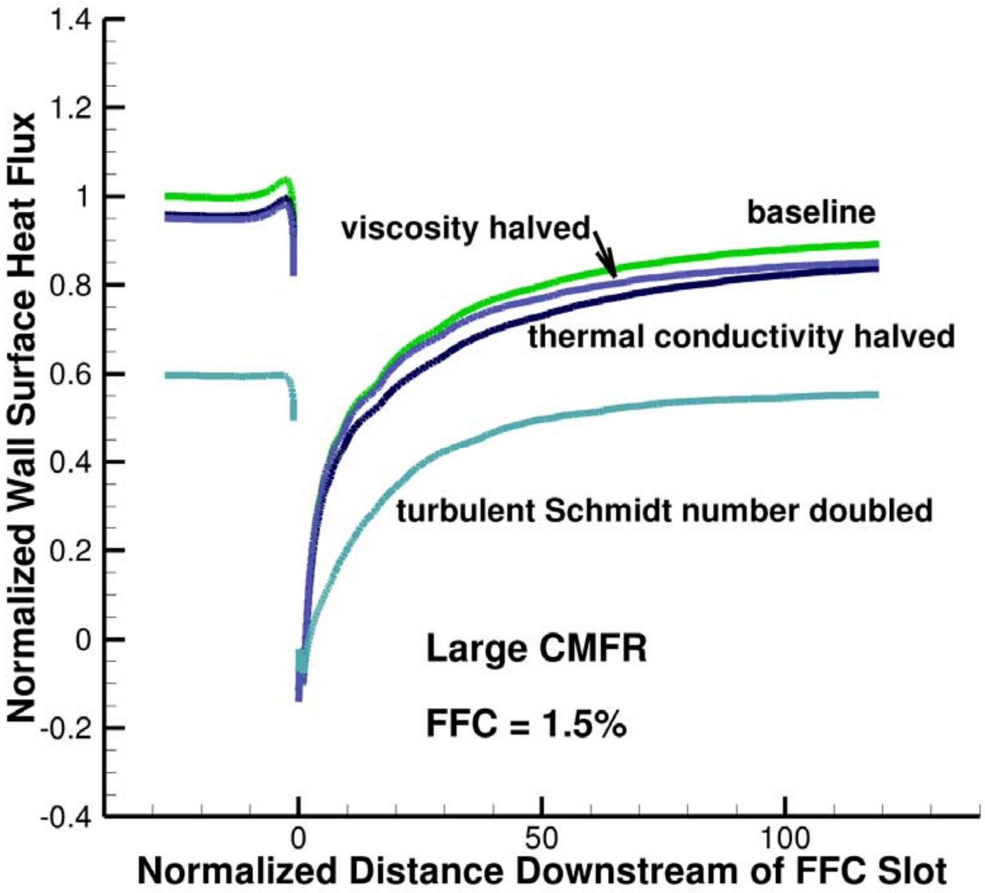

**Wall surface heat flux greatly reduced by halving turbulent mass diffusivity (prescribed by selecting turbulent Schmidt number in the model)**

# Summary

- A model was assembled to simulate hydrocarbon FFC
- The model consists of steady-state compressible flow RANS equations, with a SST k-ω turbulence model, conjugate and radiative heat transfer, with equilibrium chemistry in a conserved scalar formulation
- Validation was attempted using lab-scale experimental wall heat flux data
- Sensitivity studies were performed to identify influential model parameters and key unaccounted-for physics

# Conclusions

- The simulations predicted trends in the solution behavior that are consistent with the included physics models
- The simulations predicted greater heat flux reduction than experiment immediately downstream of the FFC slot
- Everywhere else, the simulations predicted much smaller heat flux reduction than observed in experiment
- The simulations showed that under the experimental conditions, radiative heat transfer is comparable to convection
- The simulations showed that the carbon deposits on the walls are a likely cause for the observed small fluxes
- The simulations also showed that a lower turbulent mass diffusivity may help explain observed small fluxes

# Planned Research

- Inclusion of thermal radiation in the model, with improved model parameter values
- Refined model for the turbulent Schmidt number
- Inclusion of non-equilibrium kerosene pyrolysis chemistry through flamelet or finite-rate chemistry approach
- Inclusion of chemistry and physics for soot formation, oxidation, transport and deposit on wall; thermal barrier
- Interaction between successive FFC slot flows

# Questions?

AIR FORCE RESEARCH LABORATORY

# Backup Slides

## Slides with additional information

# Mesh near Slot

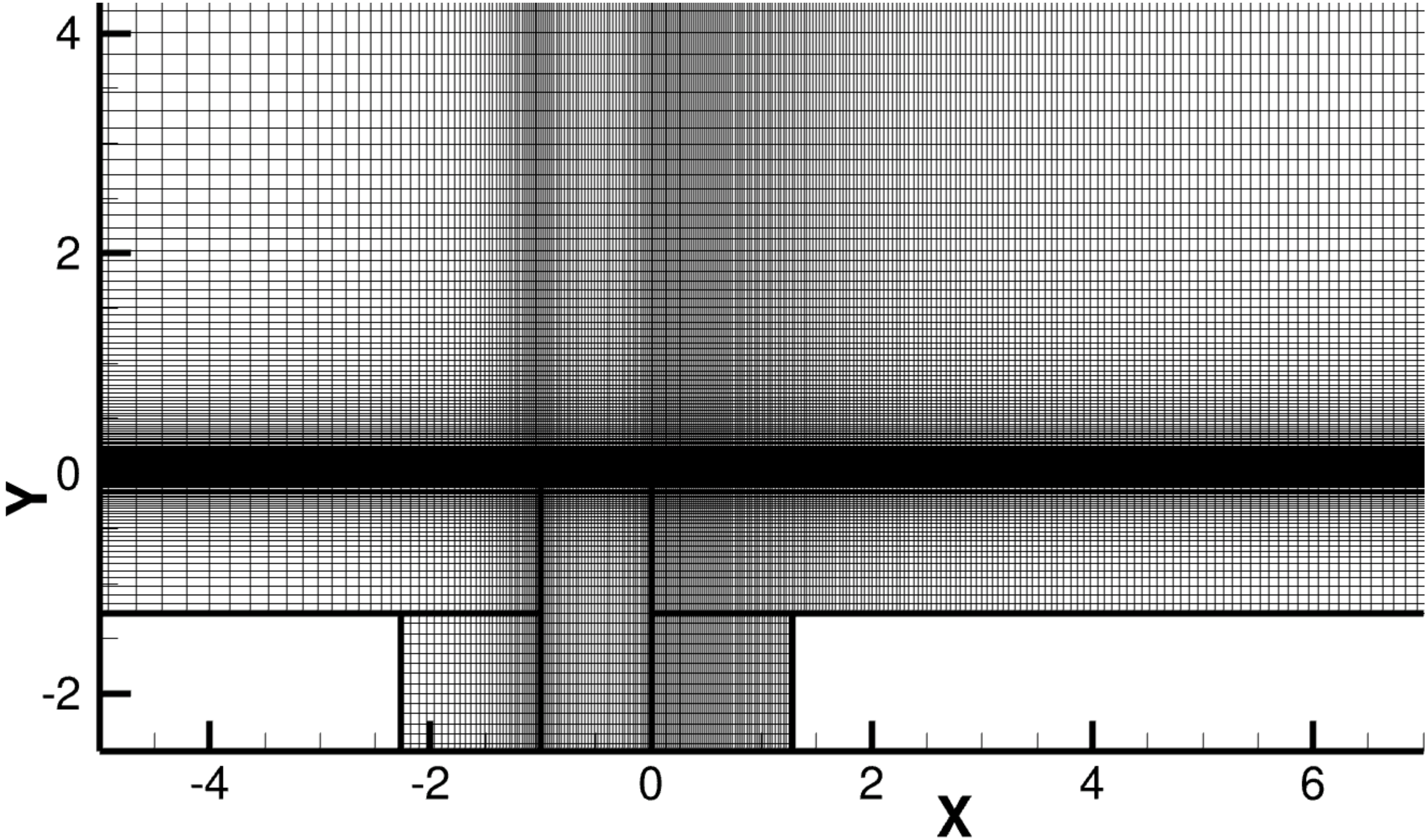
4
2
0
-2
Y
-4
-2
0
2
4
6
X

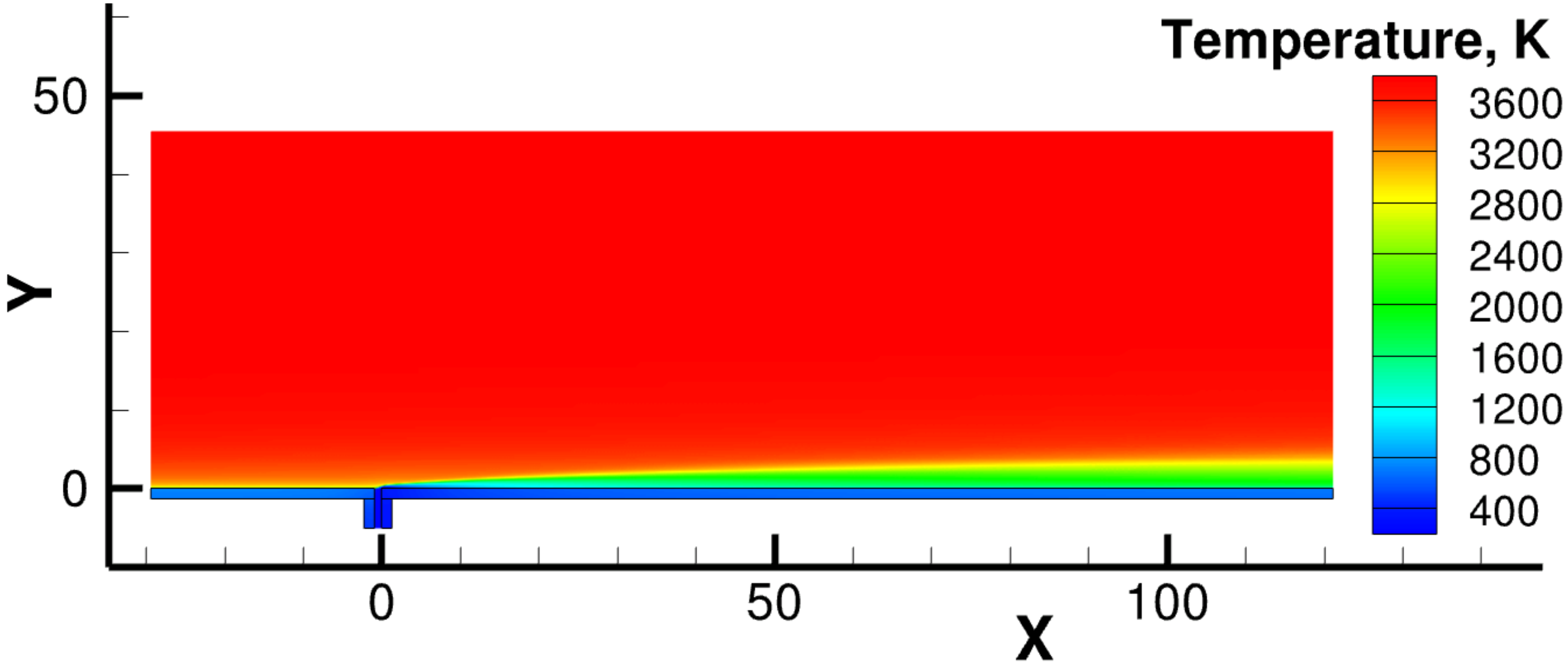
Temperature, K
3600
3200
2800
2400
2000
1600
1200
800
400
50
0
Y
0
50
100
X

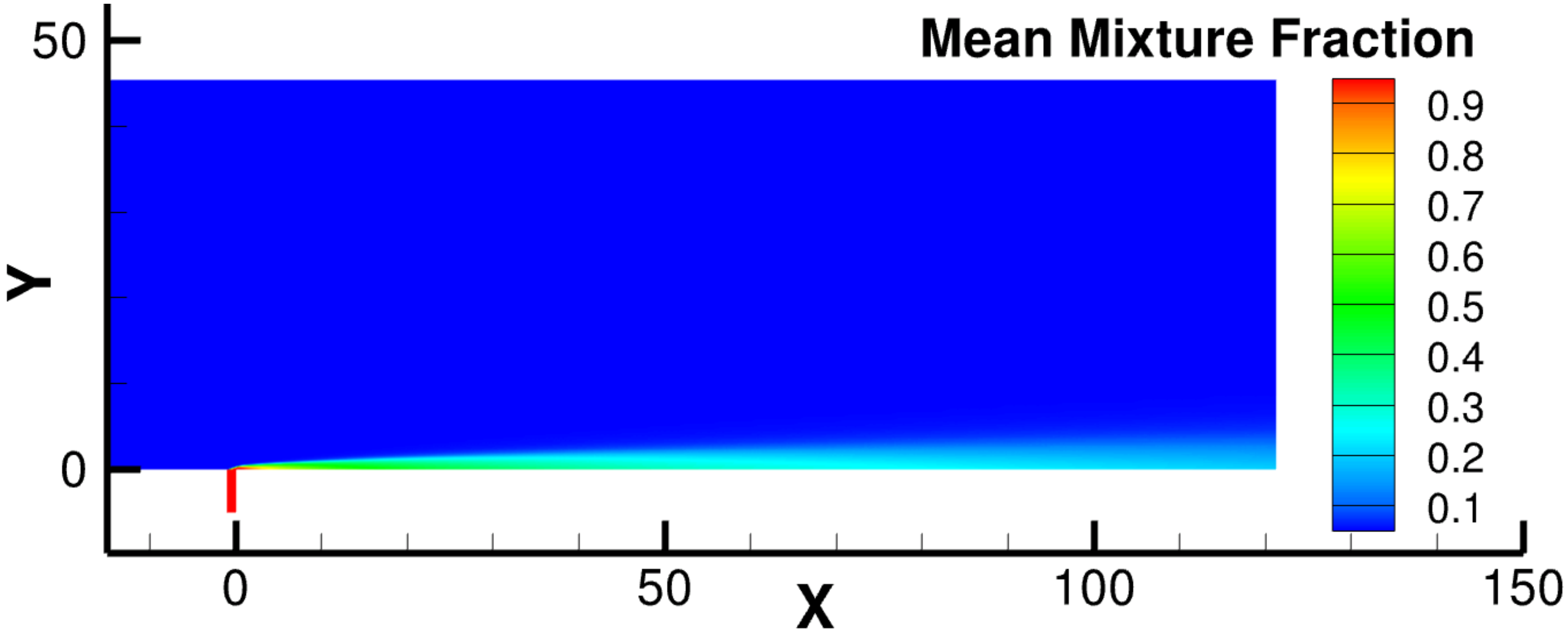
Mean Mixture Fraction
0.9
0.8
0.7
0.6
0.5
0.4
0.3
0.2
0.1
50
0
Y
0
50
100
150
X

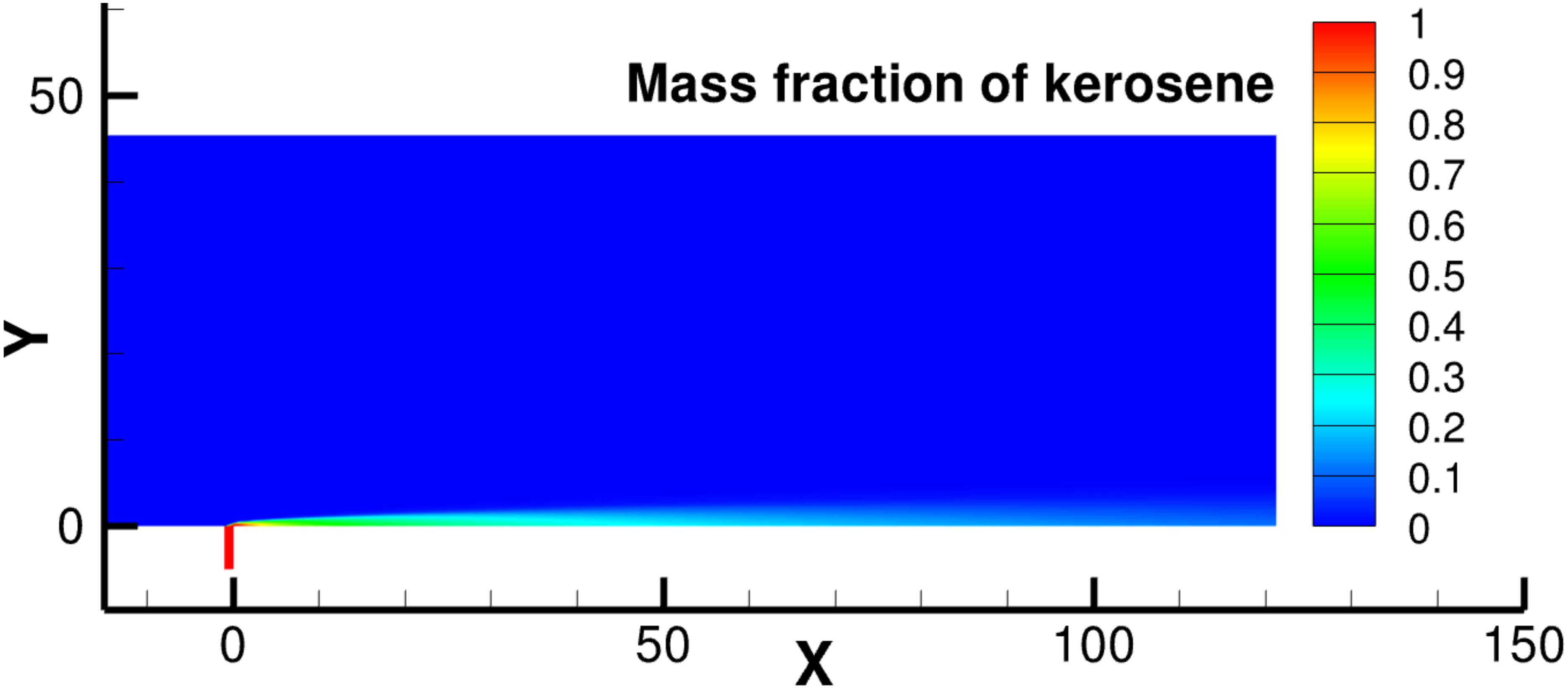
Mass fraction of kerosene
1
0.9
0.8
0.7
0.6
0.5
0.4
0.3
0.2
0.1
0
Y
50
0
X
0
50
100
150

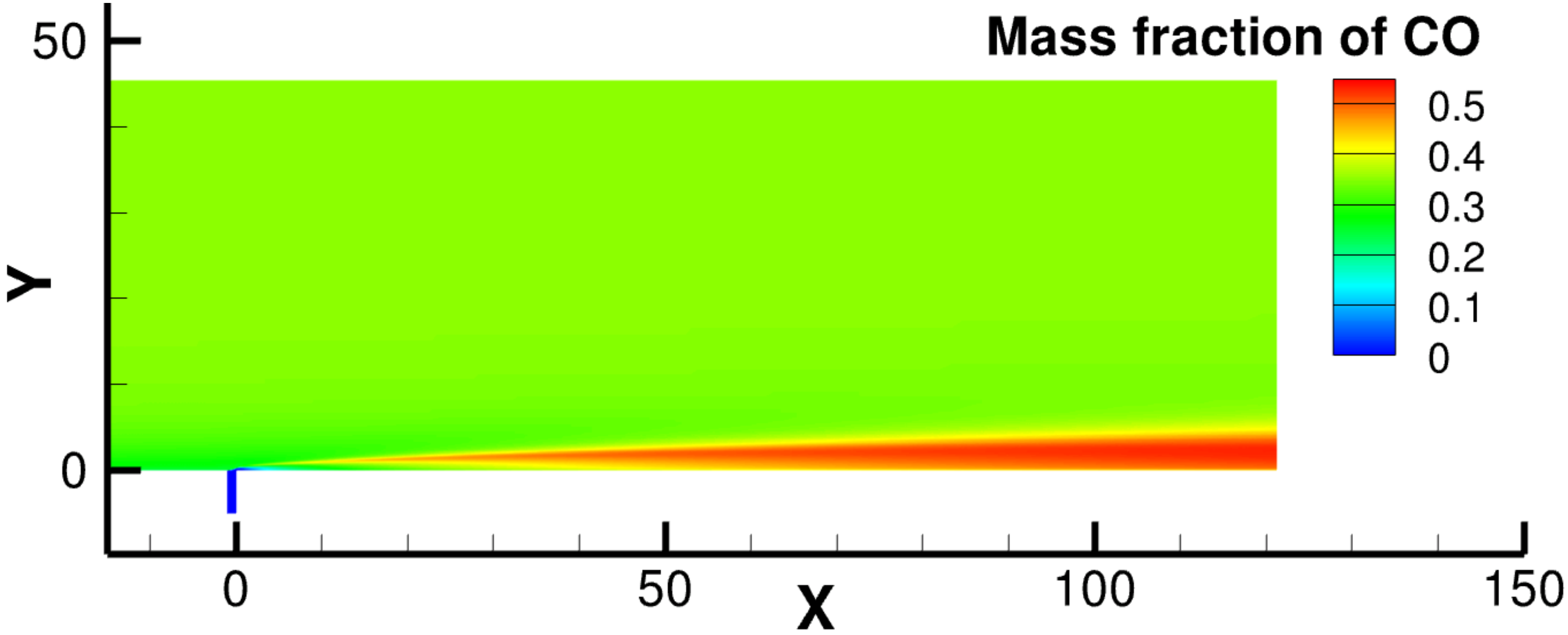
Mass fraction of CO
0.5
0.4
0.3
0.2
0.1
0
50
0
Y
0
50
100
150
X

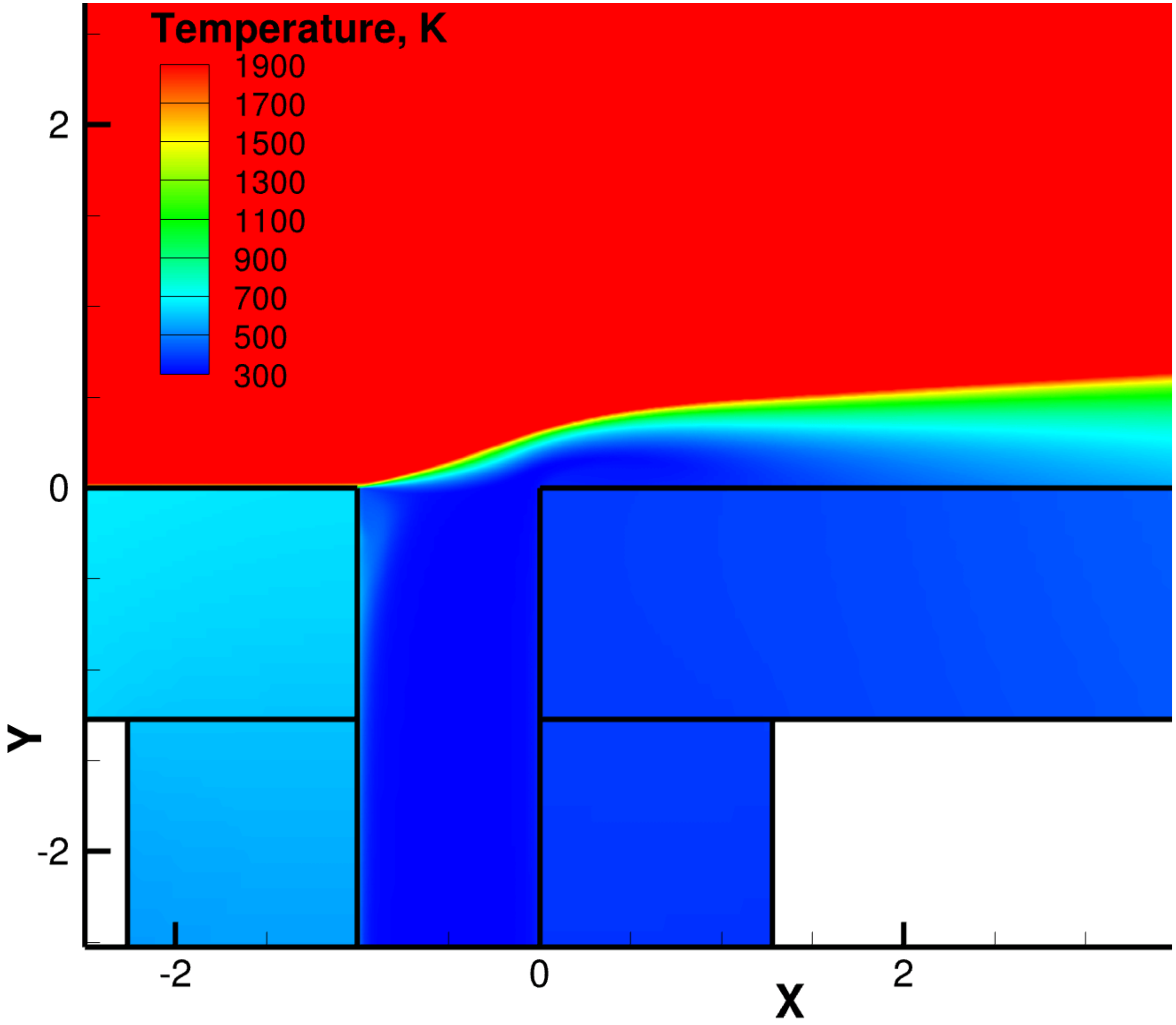
Temperature, K
1900
1700
1500
1300
1100
900
700
500
300
2
0
-2
Y
-2
0
2
X

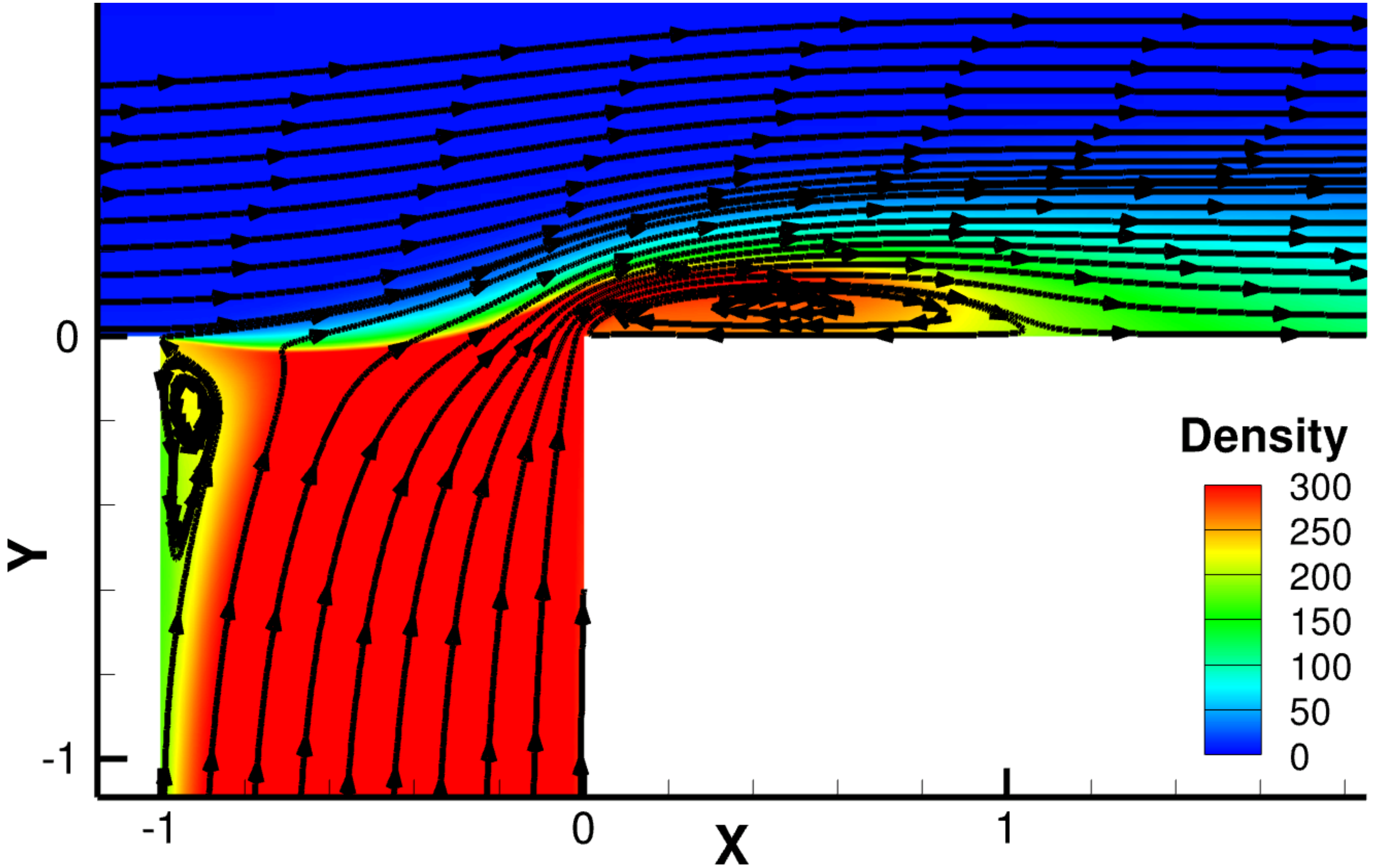
0
-1
Y
-1
0
1
X
Density
300
250
200
150
100
50
0

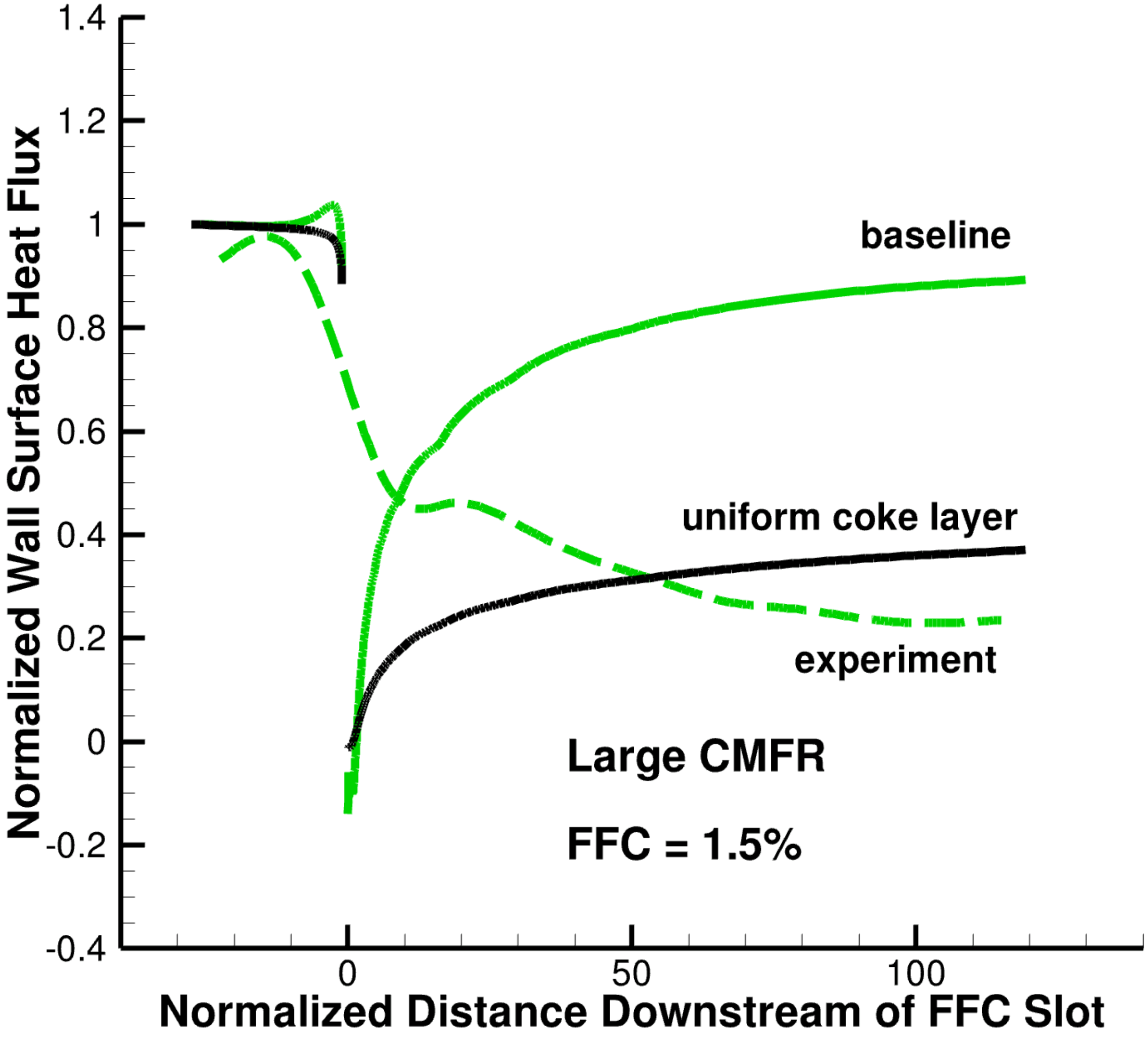

DISTRIBUTION STATEMENT A. Approved for Public Release; Distribution Unlimited.

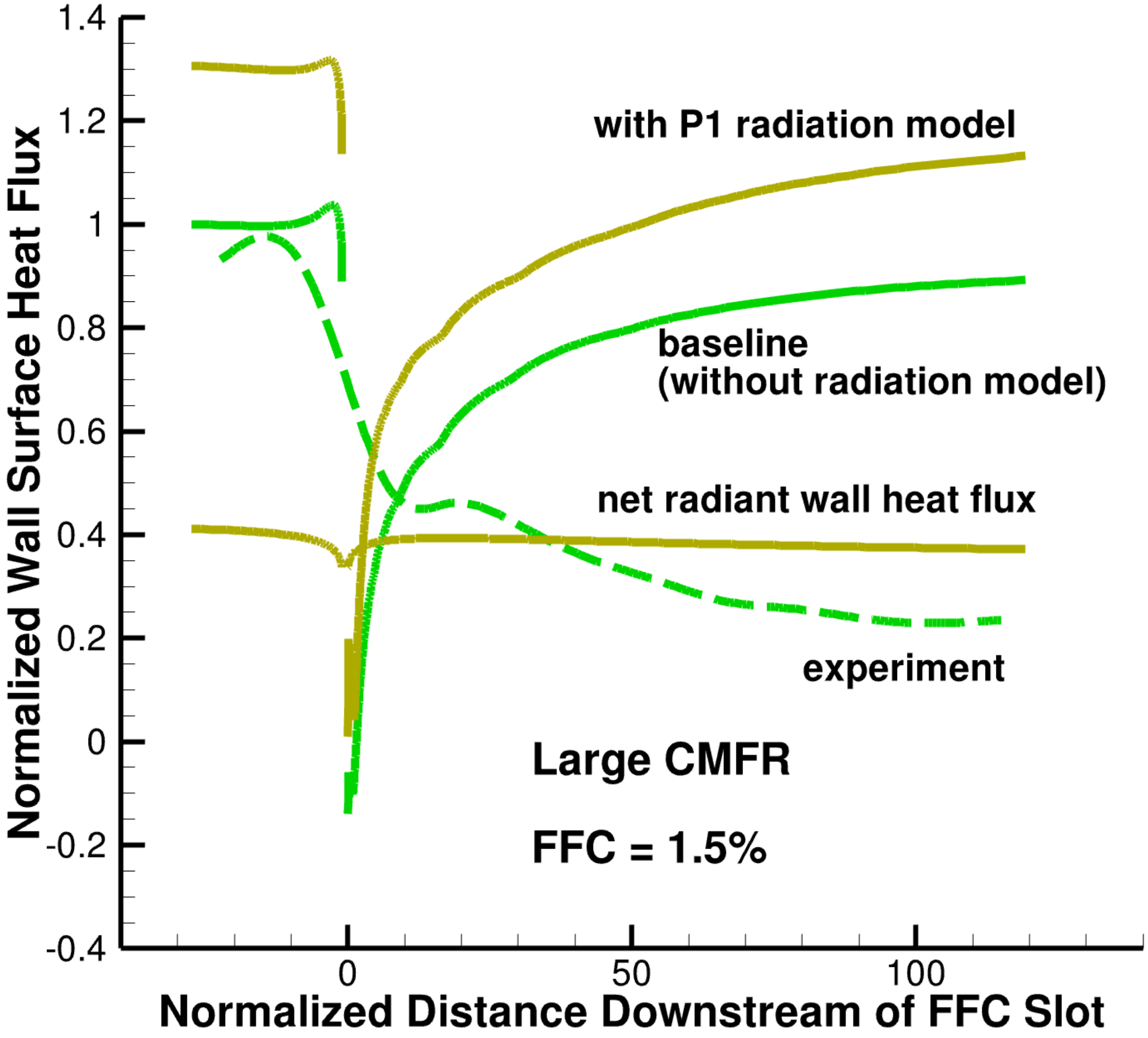

Normalized Wall Surface Heat Flux
1.4
1.2
1
0.8
0.6
0.4
0.2
0
-0.2
-0.4
0
50
100
Normalized Distance Downstream of FFC Slot
with P1 radiation model
baseline
(without radiation model)
net radiant wall heat flux
experiment
Large CMFR
FFC = 1.5%

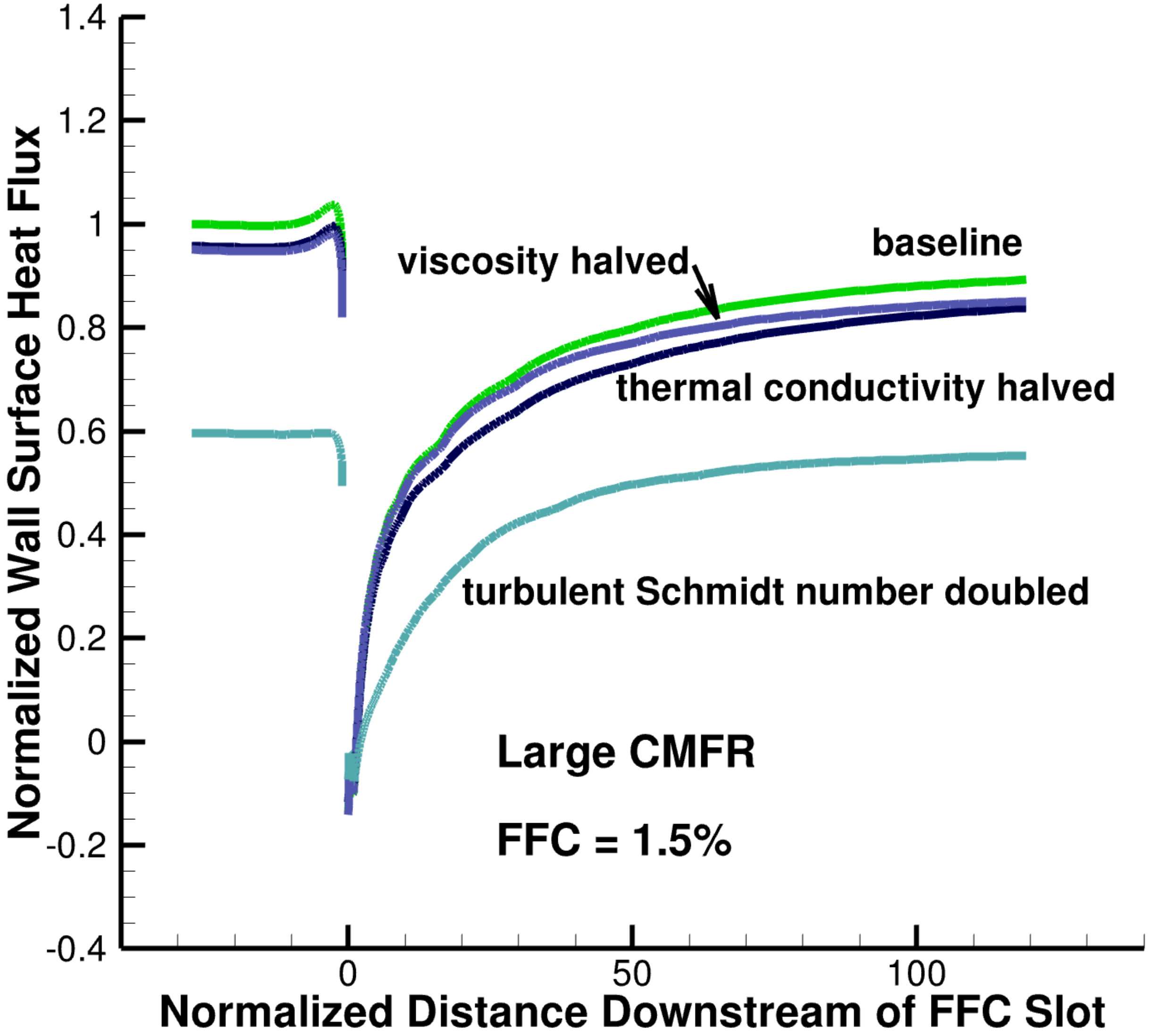

1.4
1.2
1
0.8
0.6
0.4
0.2
0
-0.2
-0.4
Normalized Wall Surface Heat Flux
0
50
100
Normalized Distance Downstream of FFC Slot
viscosity halved
baseline
thermal conductivity halved
turbulent Schmidt number doubled
Large CMFR
FFC = 1.5%

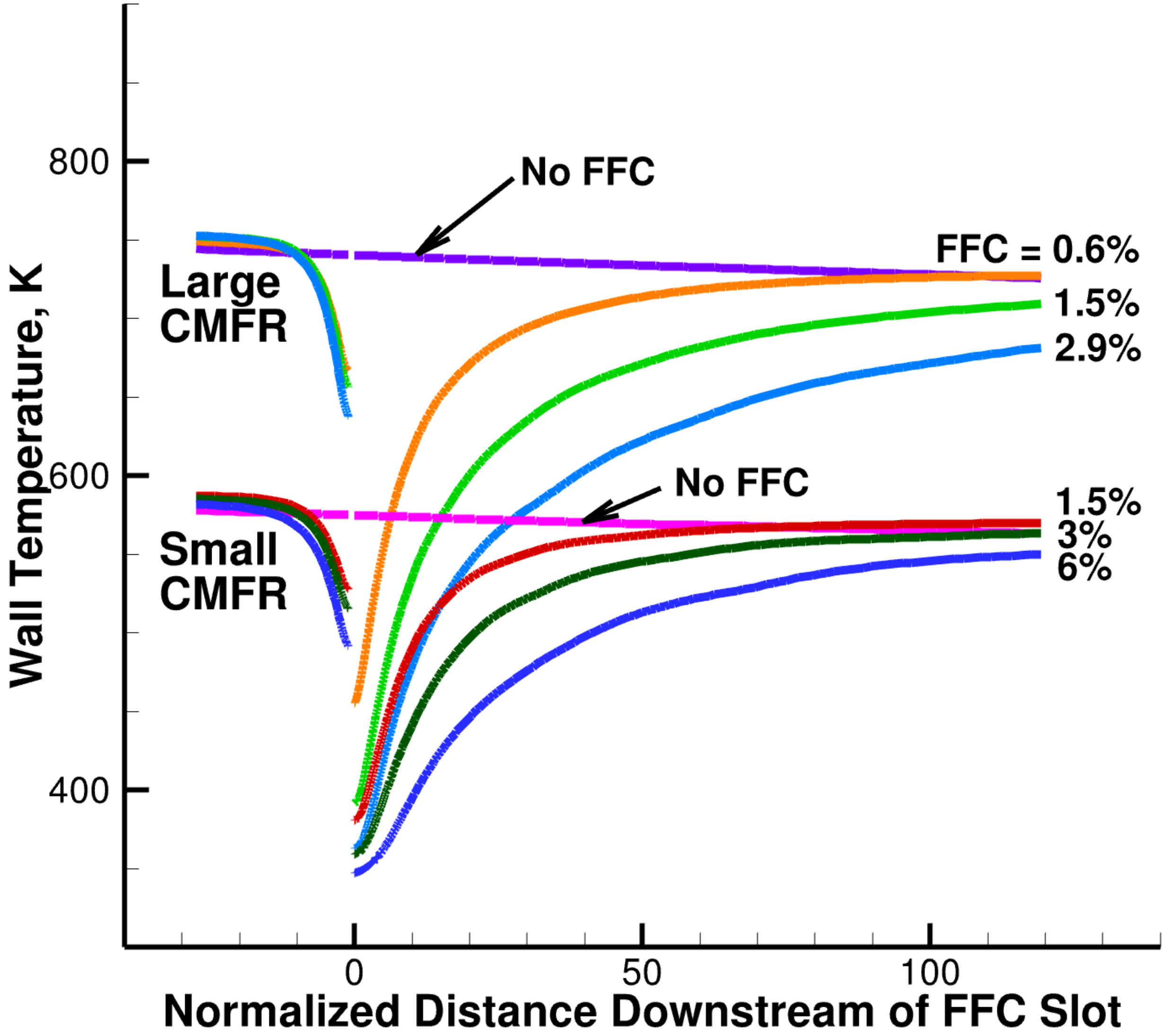
Wall Temperature, K
800
600
400
0
50
100
Normalized Distance Downstream of FFC Slot
No FFC
FFC = 0.6%
1.5%
2.9%
Large CMFR
No FFC
1.5%
3%
6%
Small CMFR

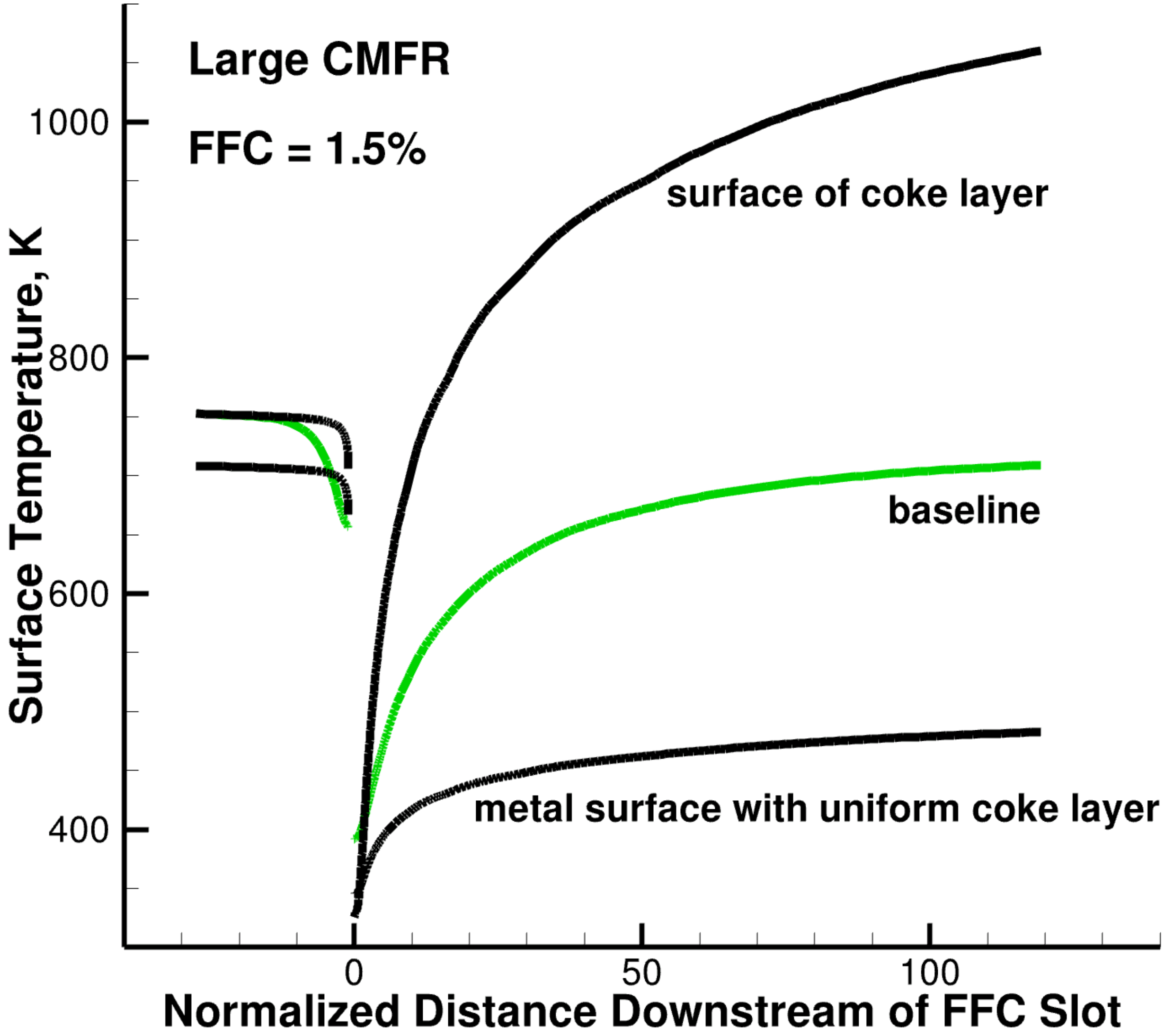
Large CMFR
FFC = 1.5%
surface of coke layer
baseline
metal surface with uniform coke layer
Surface Temperature, K
1000
800
600
400
0
50
100
Normalized Distance Downstream of FFC Slot

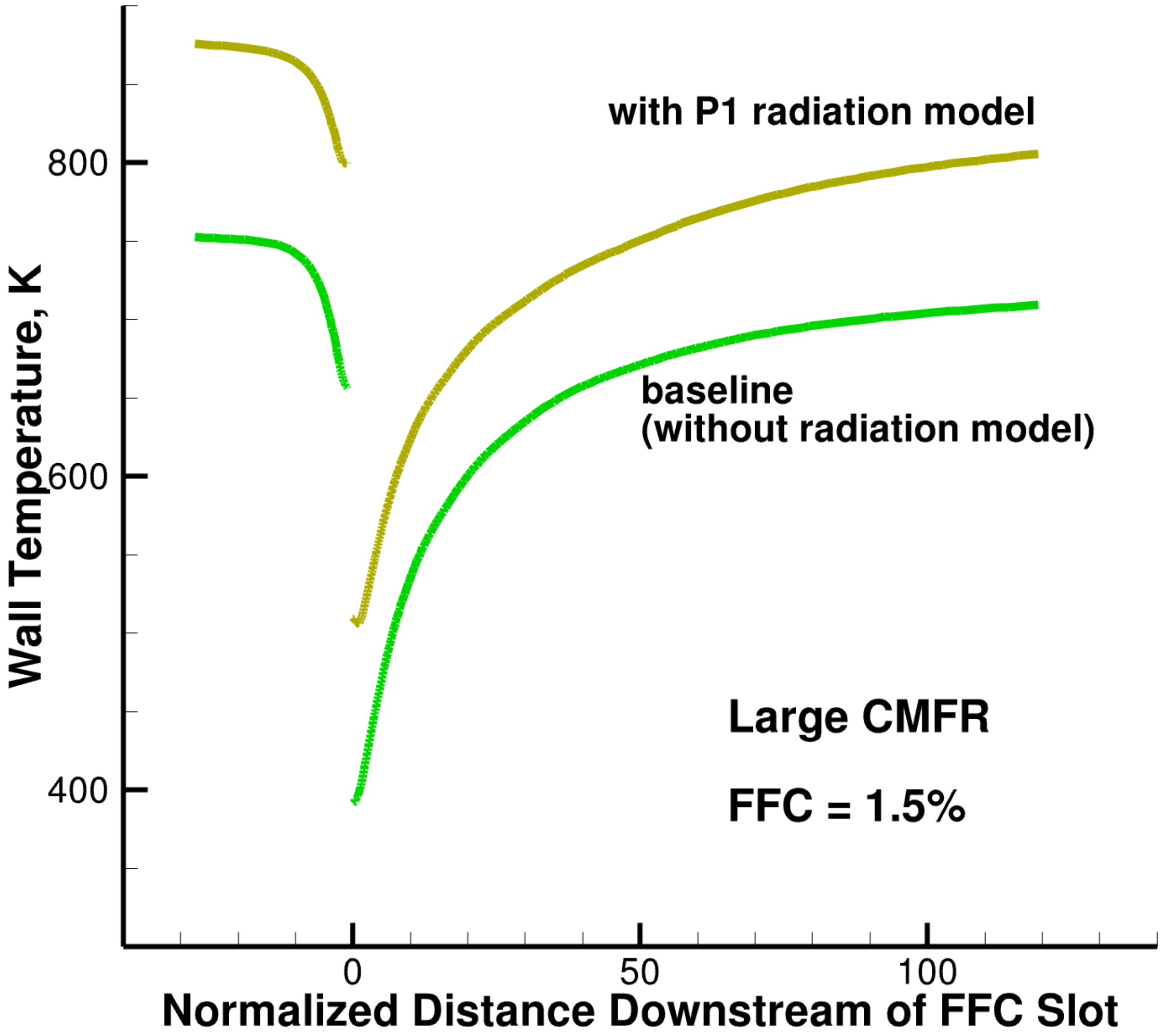
with P1 radiation model
baseline
(without radiation model)
Large CMFR
FFC = 1.5%
800
600
400
Wall Temperature, K
0
50
100
Normalized Distance Downstream of FFC Slot

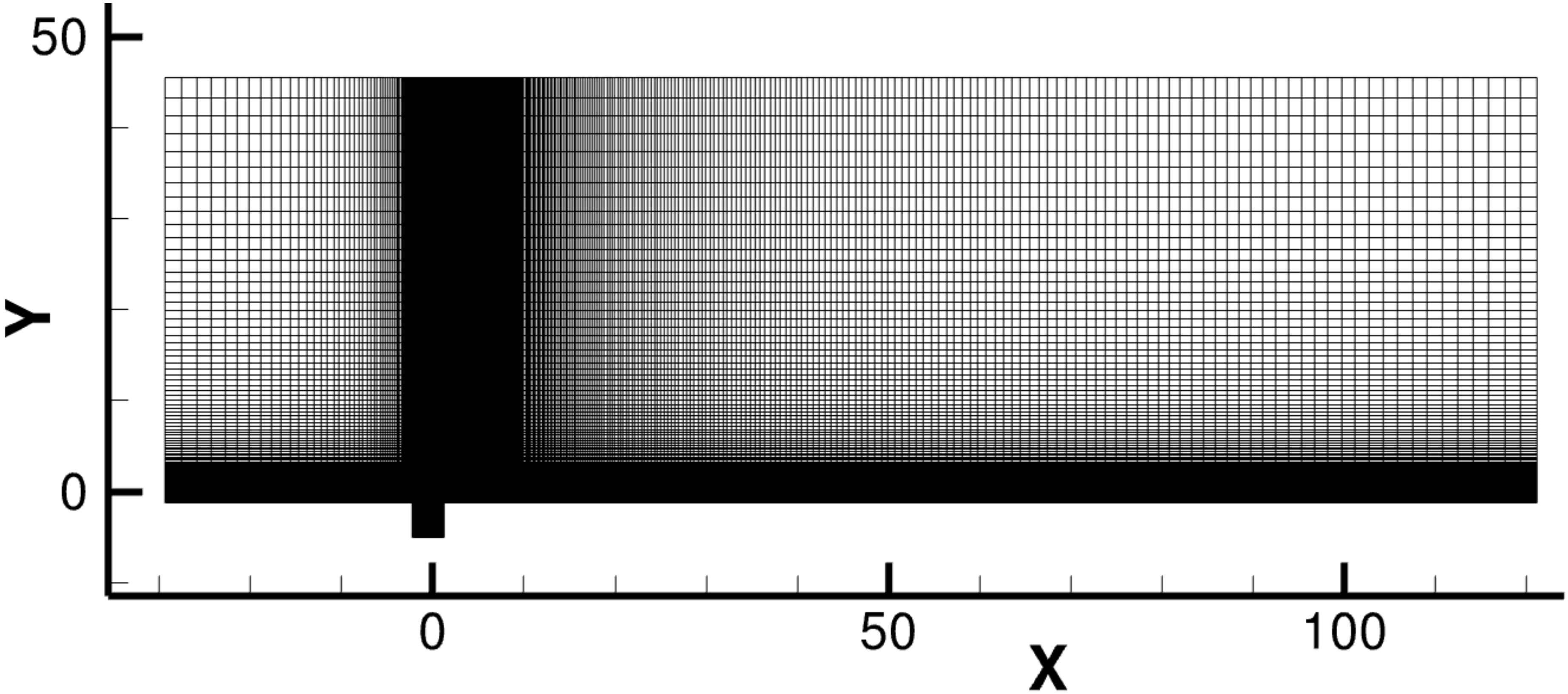
50
0
Y
0
50
100
X

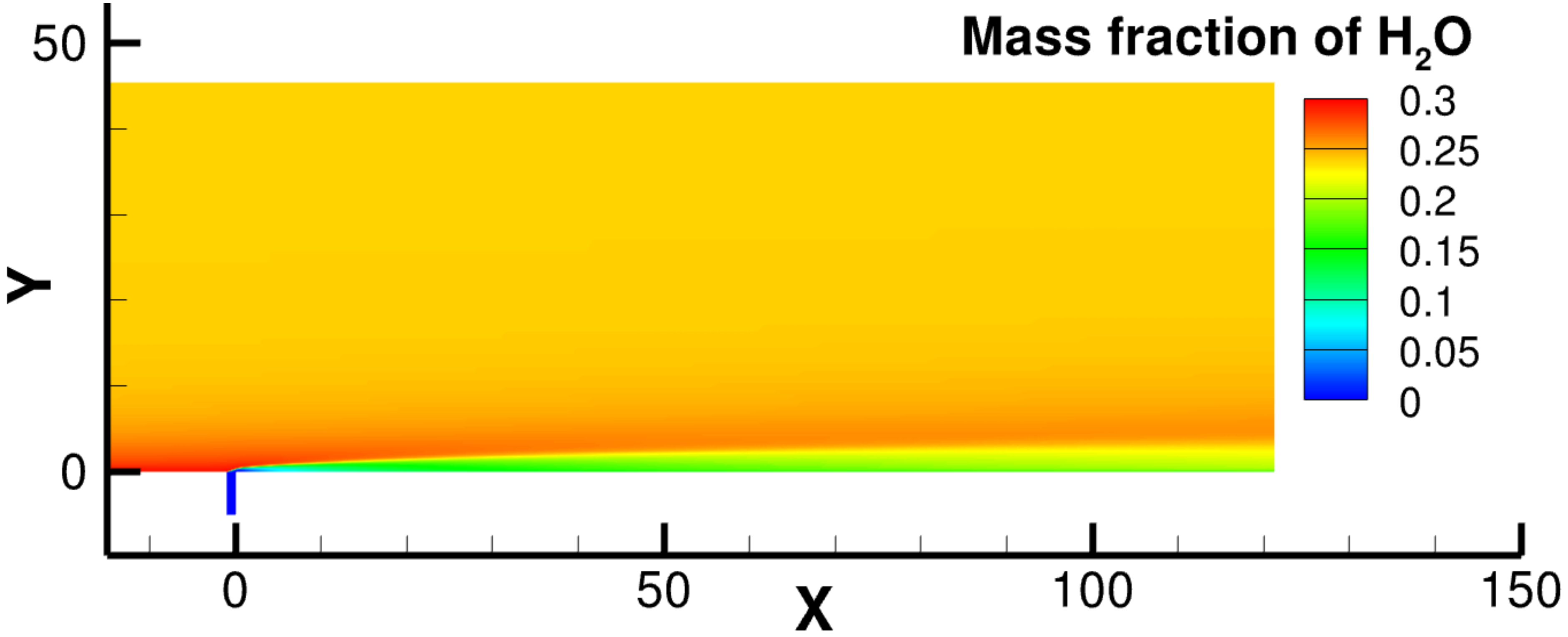
Mass fraction of $H_2O$
0.3
0.25
0.2
0.15
0.1
0.05
0
50
0
Y
0
50
100
150
X

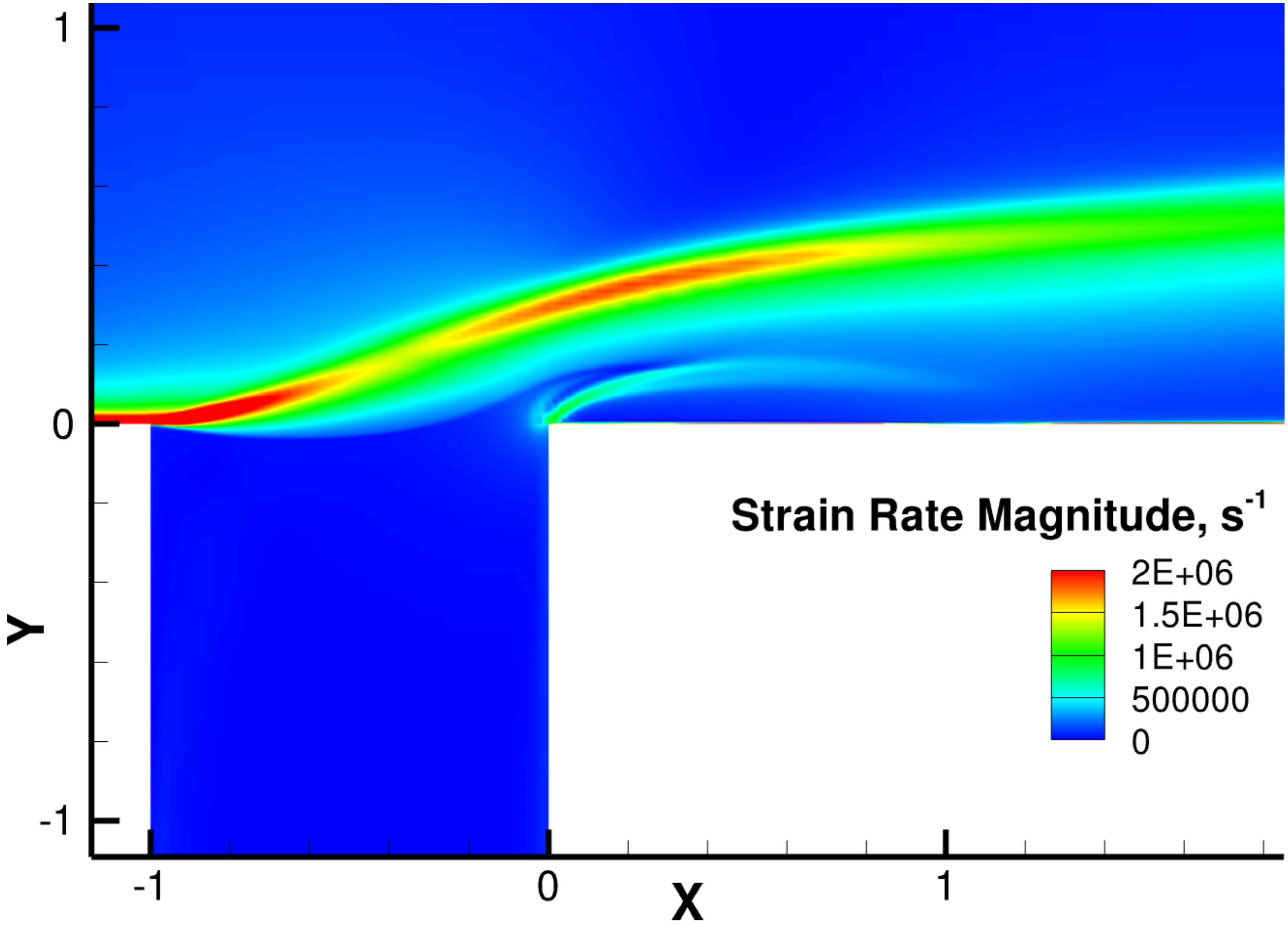
1
0
-1
Y
-1
0
X
1
Strain Rate Magnitude, s$^{-1}$
2E+06
1.5E+06
1E+06
500000
0

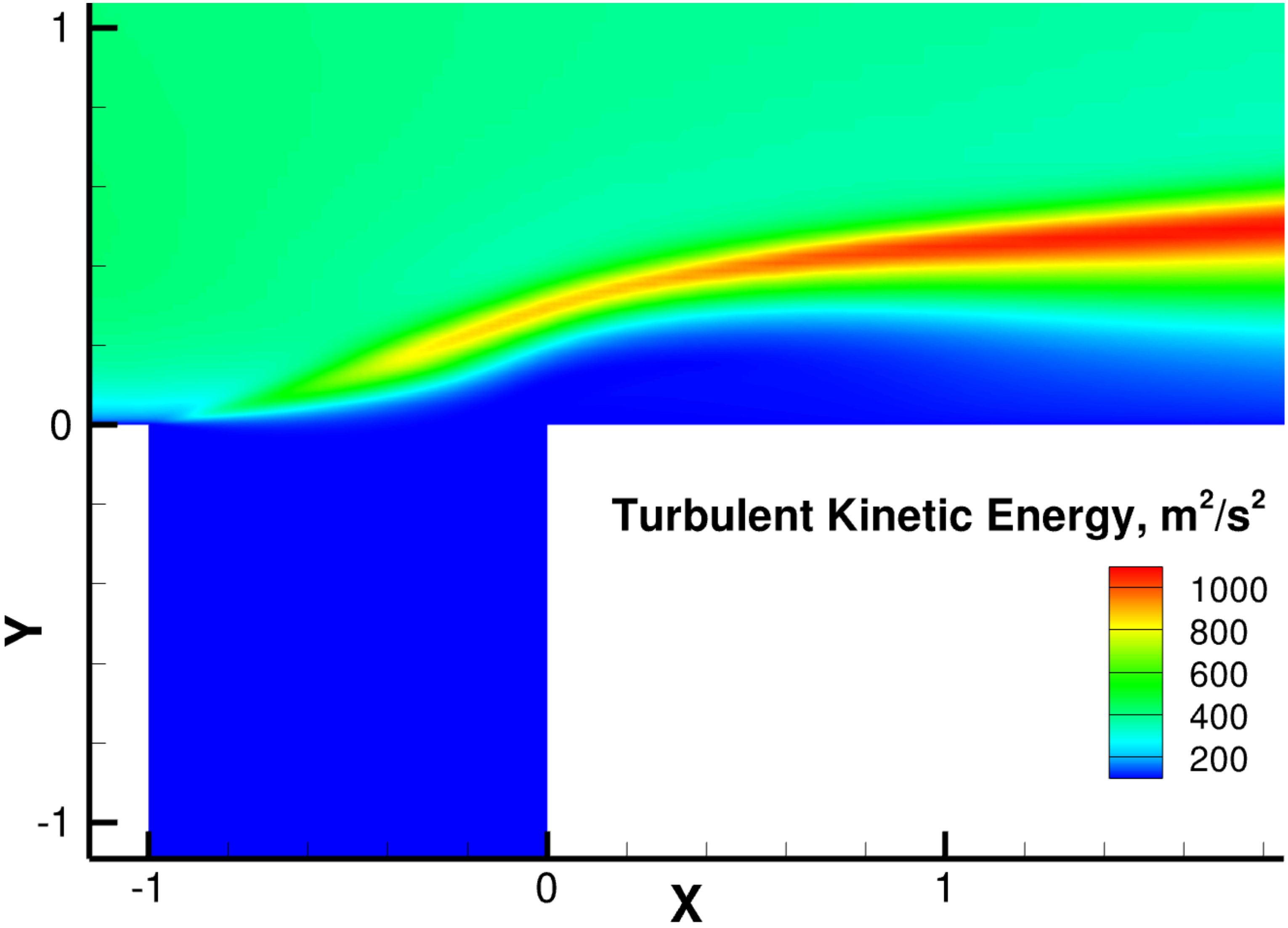
Turbulent Kinetic Energy, m²/s²
1000
800
600
400
200
1
0
-1
Y
-1
0
1
X

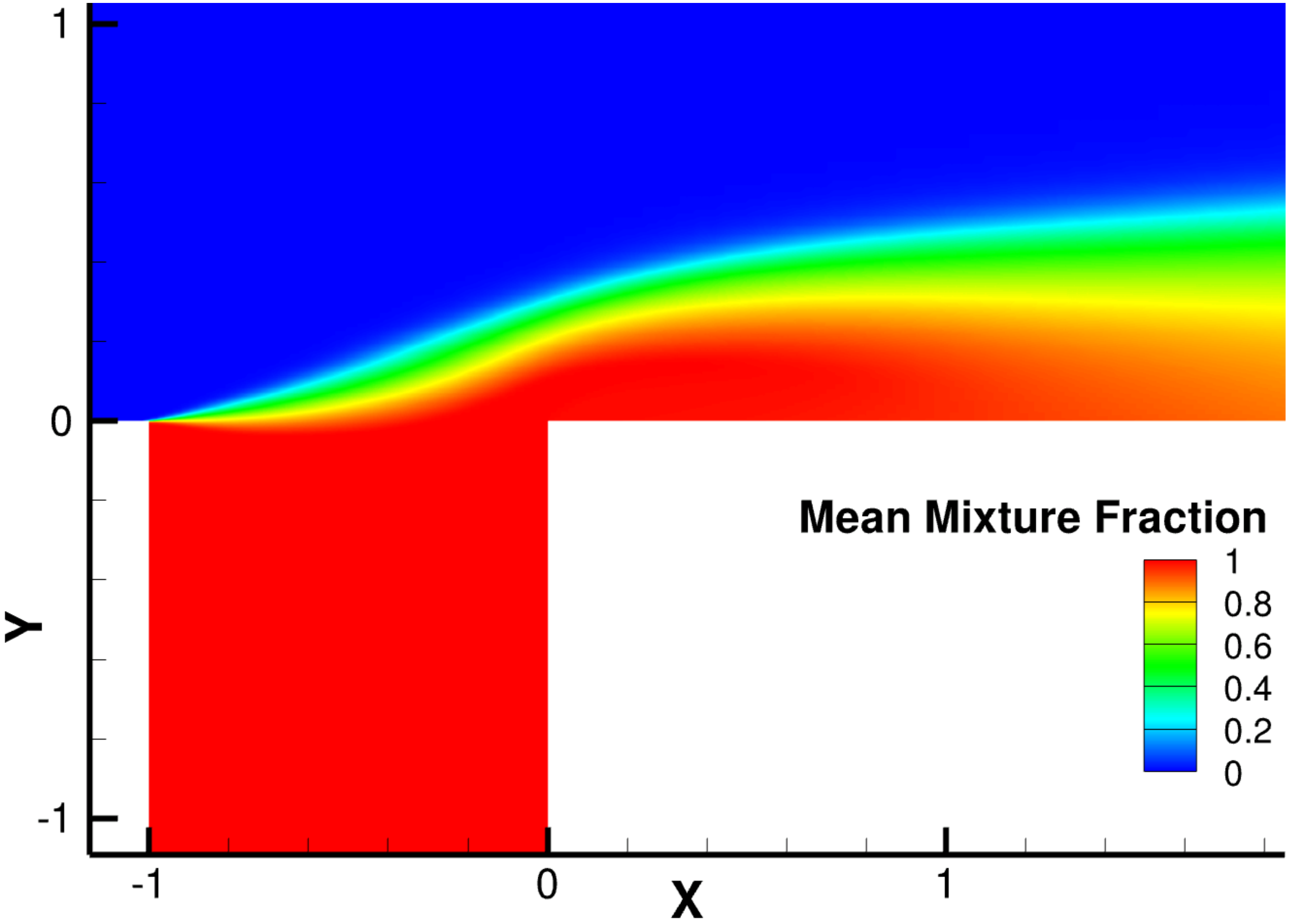
Mean Mixture Fraction
1
0.8
0.6
0.4
0.2
0
Y
1
0
-1
X
-1
0
1

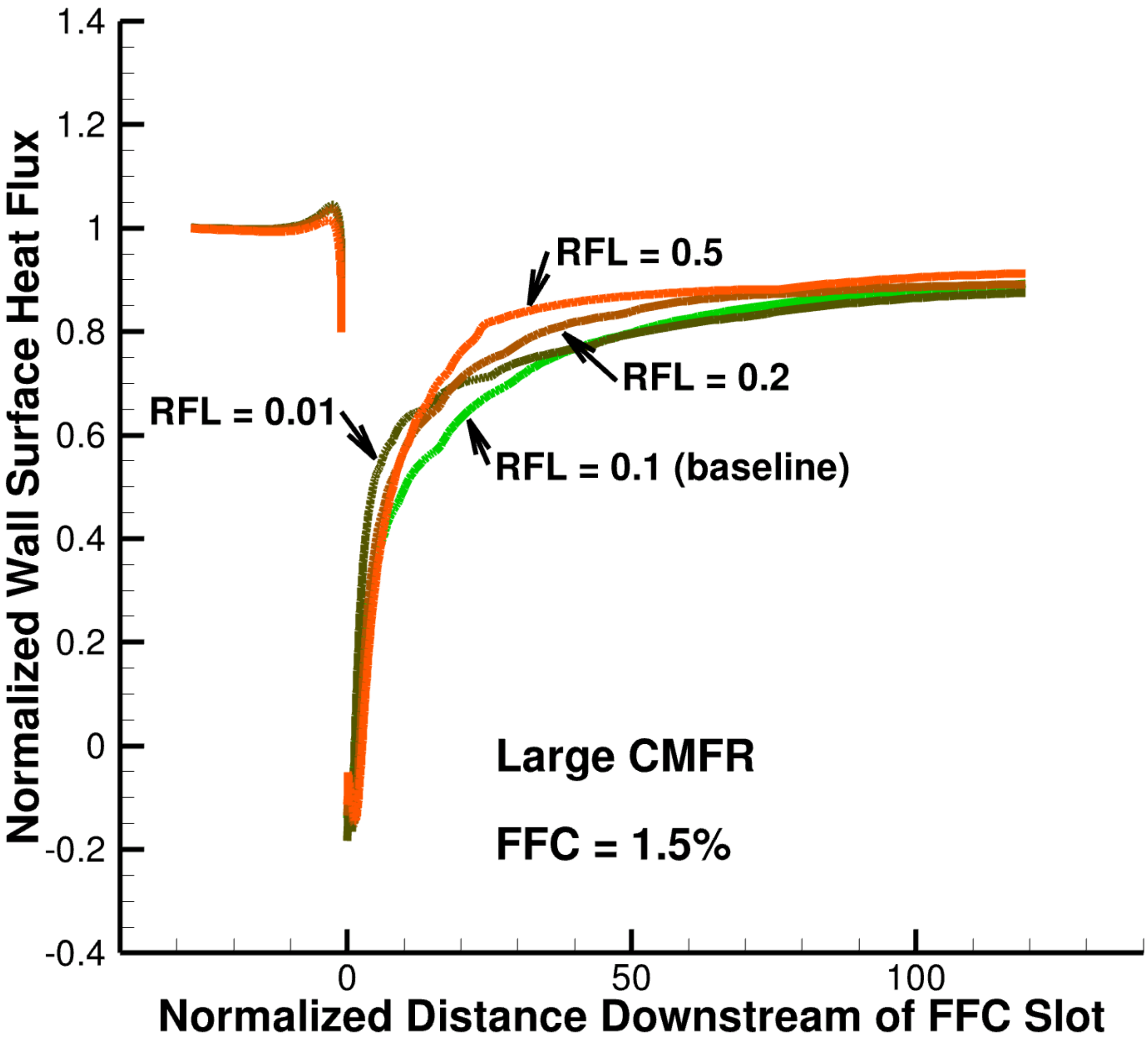
1.4
1.2
1
0.8
0.6
0.4
0.2
0
-0.2
-0.4
Normalized Wall Surface Heat Flux
0
50
100
Normalized Distance Downstream of FFC Slot
RFL = 0.5
RFL = 0.2
RFL = 0.01
RFL = 0.1 (baseline)
Large CMFR
FFC = 1.5%

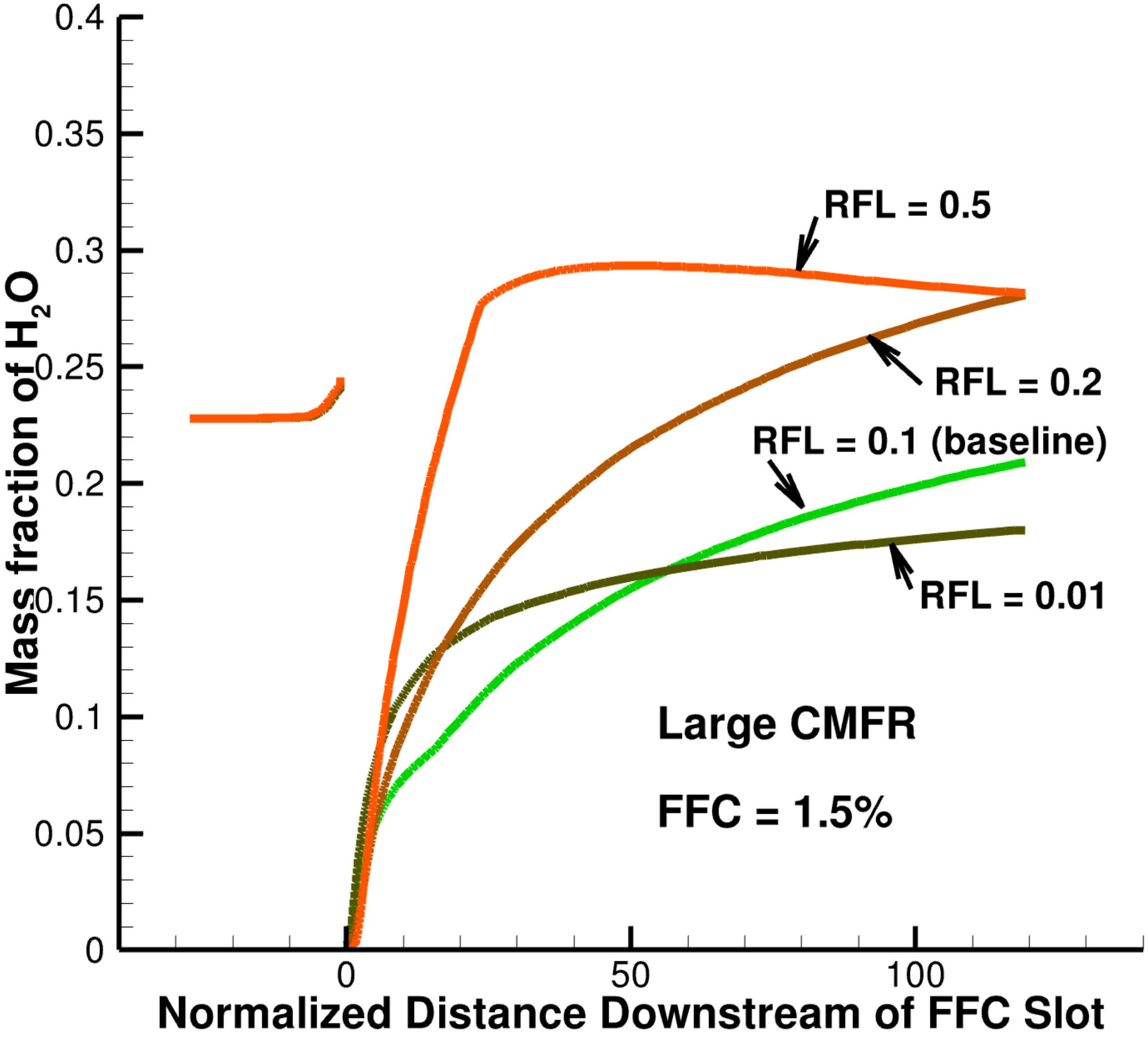

DISTRIBUTION STATEMENT A. Approved for Public Release; Distribution Unlimited.

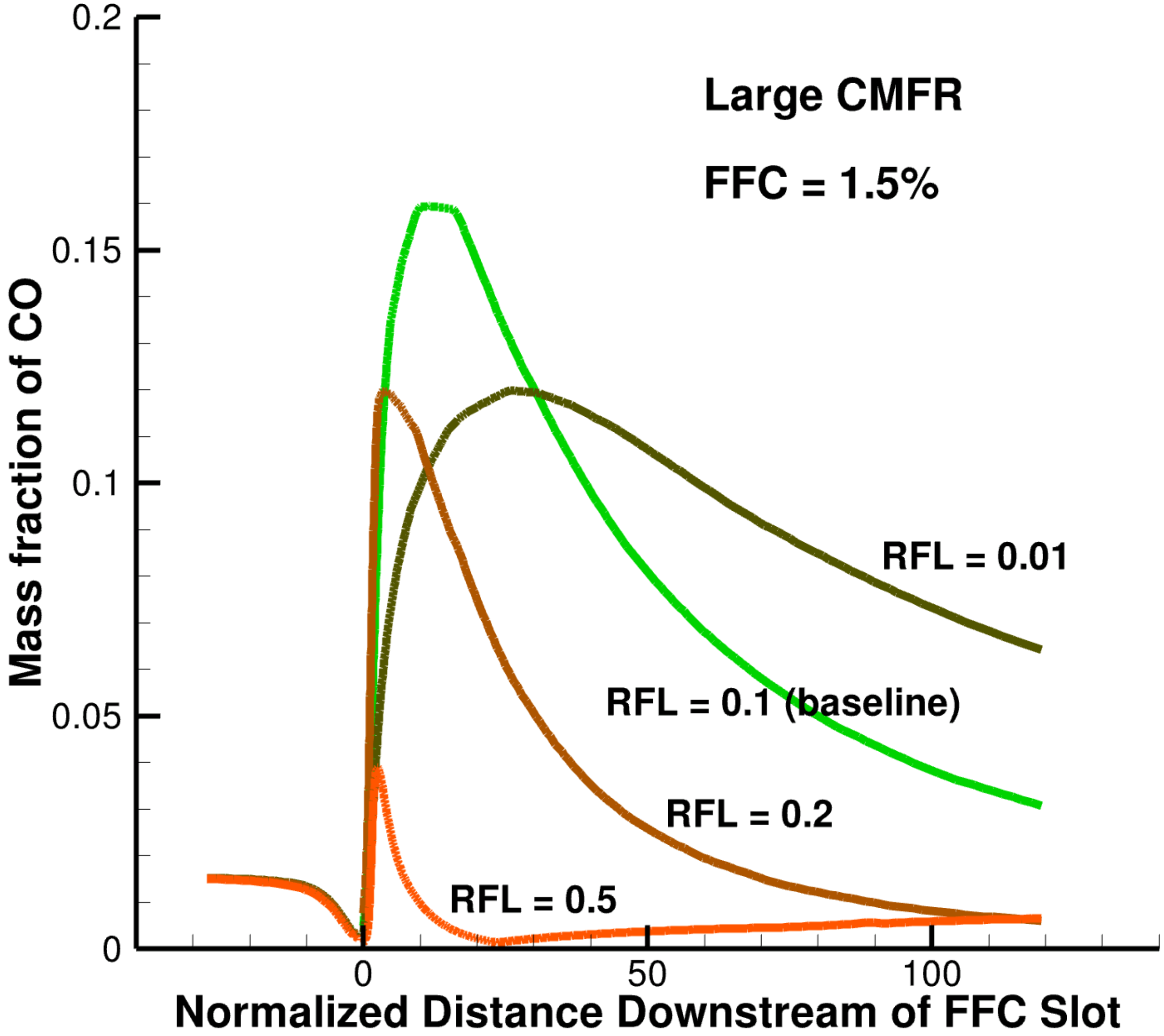
Large CMFR
FFC = 1.5%
RFL = 0.01
RFL = 0.1 (baseline)
RFL = 0.2
RFL = 0.5
Mass fraction of CO
0.2
0.15
0.1
0.05
0
0
50
100
Normalized Distance Downstream of FFC Slot